LATTICE BOLTZMANN METHOD AND IMMISCIBLE TWO-PHASE FLOW

A Thesis
Presented to
The Academic Faculty

by

Guillaume Rannou

In Partial Fulfillment
of the Requirements for the Degree
Master of Science in the
School of School of Mechanical Engineering/Paper Science and Engineering

Georgia Institute of Technology
December 2008

LATTICE BOLTZMANN METHOD AND IMMISCIBLE TWO-PHASE FLOW

Approved by:

Dr. Cyrus K. Aidun, Advisor
School of Mechanical Engineering
Georgia Institute of Technology

Dr. S. Mostafa Ghiaasiaan
School of Mechanical Engineering
Georgia Institute of Technology

Dr. Marc K. Smith
School of Mechanical Engineering
Georgia Institute of Technology

Date Approved: November 13, 2008

ACKNOWLEDGEMENTS

I want to thank my advisor, Dr. Cyrus Aidun. I am grateful for his support and guidance, which has helped me at every step of my Master's thesis. It has been an honor to work under him.

I want to thank Dr. M.K. Smith and Dr. S.M. Ghiaasiaan for accepting to serve on my thesis committee and for their insightful comments.

Finally, I would like to thank my family, for believing in me and supporting me.

TABLE OF CONTENTS

LIST OF TABLES

LIST OF FIGURES

LIST OF SYMBOLS

ρ	density
e_i	lattice vectors
c	lattice velocity
w_i	weighting factors
f , g	distribution functions
Ω_i	collision operator
k	phase (k=β or k=α)
τ	relaxation parameter
ν	kinematic viscosity
p	pressure
f^{eq}	equilibrium distribution function
u	velocity
r_i	coefficients for $\rho_\beta \neq \rho_\alpha$
s_i	surface tension force (color-fluid model)
κ	local curvature (color-fluid model) or surface tension coefficient (mean-field theory model)
σ	surface tension coefficient
VOF	volume of fluid function
δ	fluid-separation coefficient (color-fluid model)
λ	coefficient - two-relaxation-time collision (color-fluid model)
V_{inter}	velocity on the outer side of the interface
n_k	number density $n_k = \rho_k / m_k$ (interparticle-potential model)

m_k	initial density (interparticle-potential model)
u^{eq}	modified equilibrium velocity (interparticle-potential model)
$F_k(x)$	interactive force (interparticle-potential model)
$g_{k\bar{k}}$	coupling constant (interparticle-potential model)
N_k	number of nodes in the k–layer (interparticle-potential model)
F	free-energy density (free-energy model)
μ	chemical potential (free-energy model)
P_{kl}	pressure tensor(free-energy model)
n	total number density (free-energy model)
φ	number density difference between the two fluids (free-energy model)
ϕ	order parameter (free-energy model)
ϕ^*	expected order parameter (free-energy model)
F_s	surface tension force (mean-field theory model)
T	bulk temperature
R	gas constant
$\psi(\phi)$	function used in the discrete evolution equations (mean-field theory model)
H	width of the channel
μ	dynamic viscosity
$\psi(\phi)$	function used in the discrete evolution equations (mean-field theory model)
Eo	Eotvos number
Mo	Morton number
Re	Reynolds number

LIST OF ABBREVIATIONS

LBM	lattice Boltzmann method
BGK	Bhatnagar-Gross-Krook (collision operator)
VOF	volume of fluid
LSM	level set method
LG	lattice-gas
CSF	continuum surface force
EOS	equation of state
TRT	two-relaxation-time
TC	tests of coherence
PA	physical test-case compared with an analytical solution

SUMMARY

This thesis focuses on the lattice-Boltzmann method (LBM) and its ability to simulate immiscible two-phase flow. We introduce the main lattice-Boltzmann-based approaches for analyzing two-phase flow: the color-fluid model by Gunstensen, the interparticle-potential model by Shan and Chen, the free-energy model by Swift and Orlandini, and the mean-field model by He.

The first objective is to assess the ability of these methods to maintain continuity at the interface of two fluids, especially when the two fluids have different viscosities or densities. Continuity issues have been mentioned in the literature but have never been quantified. This study presents a critical comparison of the four lattice-Boltzmann-based approaches for analyzing two-phase flow by analyzing the results of the two-phase Poiseuille flow for different viscosity ratios and density ratios.

The second objective is to present the capability of the most recent version of the color-fluid model for simulating 3D flows. This model allows direct control over the surface tension at the interface. We demonstrate the ability of this model to simulate surface tension effects at the interface (Laplace bubble test), stratified two-phase flows Poiseuille two-phase flow), and bubble dynamics (the free rise of a bubble in a quiescent viscous fluid).

CHAPTER 1

INTRODUCTION

Multiphase flows play an important role, not only in many natural processes, but also in many engineering applications, such as flow through porous media, viscoelastic free surface flow, liquid jet, coating flow, bubble dynamics, and dendrite formation. Multiphase flows, widely used in industry, have to be properly modeled because accuracy and consistency of a multiphase model have a direct influence on the design process. Two-phase flows have been modeled with three methods: the volume of fluid (VOF), the level set (LSM), and the front tracking methods. These methods describe both phases with one set of equations and use a separate equation to simulate the behavior of the interface. The main problems with these techniques are that the short interactions between the two fluids are difficult to model. The lattice Boltzmann method (LBM), which is considered an alternative approach, appears to be very promising because it is easy to code, to implement, and to parallelize. In addition, being a "particle method," the LBM can easily include interfacial phenomena. The methods developed by Gunstensen et al. [1] (color-fluid model), Shan and Chen [2, 3] (interparticle-potential model), Swift et al. [4] (free-energy model), and He et al. [5] (mean-field theory model) are the four main lattice-Boltzmann-based approaches for analyzing two-phase flow.

The color-fluid model developed by Gunstensen (1991) [1] is based on the two-component lattice-gas (LG) model proposed by Rothman & Keller (1988) [6] and has been modified by Grunau et al. (1993) [7] to allow variations of density and viscosity. The color-fluid model is based on the following three concepts: red and blue particle

distribution functions $f_i^{\alpha}(x,t)$ and $f_i^{\beta}(x,t)$ represent two different fluids, the effect of surface tension is obtained through a perturbation step modeled by a collision operator added to the original collision operator, and phase separation is maintained through a segregation step by encouraging particles to go toward a region of the same color. Recent publications proposed some improvements on the Gunstensen method. Reis and Philips [8] modified the original color-fluid model by adjusting the two-phase flow operator in order to recover the single-phase Navier-Stokes equations. Lishchuk [9] used the concept of continuum surface force (CSF) to model surface tension whose effects are directly applied at the interface; therefore, it gives direct control over the surface tension value. Latva-Kokko [10] proposed a diffusion scheme that solves the lattice pinning problem and creates a symmetric distribution of particles around the interface.

The interparticle-potential model proposed by Shan and Chen [2, 3] is based on the concept of nearest-neighbor interaction. Although the original model uses *S* different particle-distribution functions to model *S* different components, we restrict this study to two components. To model interactions between these components, Shan and Chen modified the collision operator by using an equilibrium velocity, which includes an interactive force. This force guaranties phase separation and introduces surface tension effects. Several researchers [11-14] applied this model with some success. However, the authors reported some issues of accuracy which are attributed to the fact that the interface is not sharp and the model is not strictly immiscible. In order to apply the interparticle-potential model to non-ideal fluids, Yuan and Schaefer [15] and Quin [16] proposed modified interparticle-potentials to obtain a suitable equation of state (EOS). In order to control the surface tension independently of the EOS, Falcucci et al. [17] proposed a

second neighbor repulsive interaction model which has been quantitatively studied by Chibbaro et al. [18]. These improvements make the interparticle-potential model able to simulate complex flow phenomena but do not solve the continuity problem at the interface. The present paper considers the original model.

The free-energy model proposed by Swift and Orlandini [4, 19] uses a free-energy function to include surface tensions effects in a manner consistent with thermodynamics. Contrary to the two previous models, this model considers the total density ρ and the density difference $\Delta\rho$ as simulation parameters instead of the density of each phase. The two distribution functions that describe the evolution of ρ and $\Delta\rho$ are governed by the single-relaxation-time lattice-Boltzmann equation. The lack of Galilean invariance is the primary shortcoming of the original free-energy model and has been investigated, notably by Holdych et al. [20], Inamuro et al. [21] and Kalarakis et al. [22]. Zheng et al. [23] and Inamuro et al. [24] proposed two new free-energy models, which are stable for high density ratios (up to 1000). Zheng uses the convective Cahn-Hilliard equation to describe the evolution of the interface whereas Inamuro uses the pressure projection method to achieve high density ratios.

The mean-field theory model proposed by He et al. [5, 25] is valid in the nearly incompressible limits and applies to non ideal gases. In this model, the simulation parameters are the pressure and an index function, which is used to track the interface and plays the same role as the density difference in the free-energy model. Interfacial dynamics is modeled by introducing molecular interaction forces, which are approximated by the mean-field theory. Phase separation occurs naturally due to the instability of the supernodal curve of the phase diagram. This model can simulate with

accuracy Rayleigh-Taylor and Kelvin-Helmholtz instabilities, even with non-ideal and dense fluids [25, 26]. Lee and Lin recently proposed a model based on the mean-field theory model that is stable for high density ratios [27].

The first objective of this study is to compare the four main lattice-Boltzmann-based approaches for analyzing two-phase flow and to assess their ability to maintain continuity at the interface between two fluids. We used the two-phase Poiseuille-flow test case, analyzed the accuracy of each model, and focused on the discontinuity of the tangential velocity at the interface. We simulated several cases with different viscosity ratios and density ratios.

The second objective of this study is to present a 3D implementation of the most recent version of the color-fluid model and to assess its capability. Therefore, after presenting the details of the 3D implementation, we analyze the results of several validation test cases. This study notably shows the ability of this model to simulate surface tension effects at the interface (Laplace bubble test), stratified two-phase flows Poiseuille two-phase flow), and bubble dynamics (the free rise of a bubble in a quiescent viscous fluid).

CHAPTER 2

LATTICE-BOLTZMANN MODELS FOR IMMISCIBLE TWO PHASE FLOW

Historically, the lattice Boltzmann method (LBM) originated from the lattice-gas cellular automata (LGCA), which was introduced in 1986 by Frisch, Hasslacher and Pomeau [28]. LGCA works like a billiard game and recovers the Navier-Stokes equations in the macroscopic limit and if the lattice is sufficiently symmetric. The main motivation for developing the LBM was the desire to remove the statistical noise by replacing the Boolean particle by a density distribution function. The lattice Boltzmann is now considered a mature simulation method and has been extensively studied and reviewed [29, 30].

Single-phase lattice-Boltzmann model (D2Q9)

The lattice Boltzmann method is based on the discretization of the velocity space of the Boltzmann equations. Discretization uses a set of discrete velocity vectors that determines the geometry of the lattice. We used a D2Q9 lattice (two dimensions, nine velocities), which has the following set of discrete velocities and weighting factors:

$$e_i = \begin{cases} (0;0) & & i=0 \\ (\pm 1;0)c & (0;\pm 1)c & i=1,2,3,4 \\ (\pm 1;\pm 1)c & (\pm 1;\pm 1)c & i=5,6,7,8 \end{cases} \tag{1}$$

$$w_i = \begin{cases} 4/9 & i=0 \\ 1/9 & i=1,2,3,4 \\ 1/36 & i=5,6,7,8 \end{cases} \tag{2}$$

The dynamics of the flow is described by a distribution function f, which follows the lattice-Boltzmann equation:

$$f_i(x+c_i,t+1) = f_i(x,t) + \Omega_i(x,t) \tag{3}$$

Ω_i is the collision operator and represents relaxation to a local equilibrium state.

The equilibrium distribution function f_i^{eq} has to verify the mass conservation and the momentum conservation constraints as follows:

$$\begin{aligned} \rho &= \sum_i f_i = \sum_i f_i^{eq}, \\ \rho u &= \sum_i f_i e_i = \sum_i f_i^{eq} e_i. \end{aligned} \tag{4}$$

The following figure shows the mechanism of the LBM with the two main steps: streaming and collision.

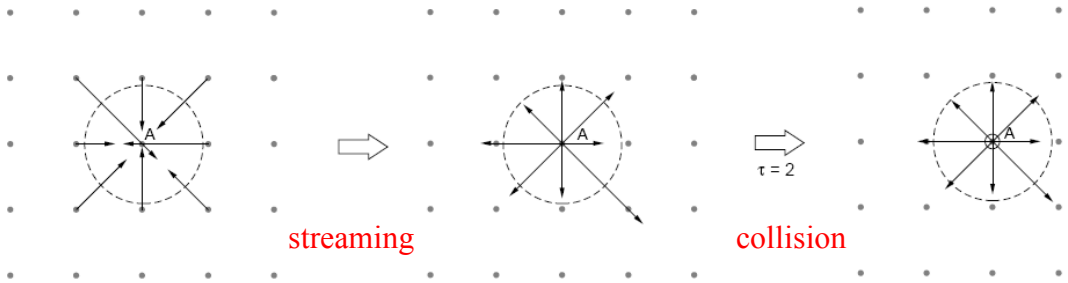

Figure 1: LBM - streaming and collision

Color fluid model

The color fluid model uses a set of two single-phase distribution functions noted f_i^k where k represents the phase (k=β or k=α). The evolution of the distribution function for each phase is described as follows.

$$f_i^k(x+e_i,t+1) = f_i^k(x,t) + \Omega_i^k(x,t) \tag{5}$$

Ω_i^k is the collision operator and represents relaxation to a local equilibrium state.

We used the Bhatnagar-Gross-Krook (BGK) collision operator:

. $$\Omega_i^k = \frac{-1}{\tau_k}\left[f_i^k - f_i^{k\ eq} \right] \tag{6}$$

The interface is implicitly defined, so the model uses only two collision operators: one collision operator for fluid α and one collision operator for fluid β. At a mixing point, the collision operator corresponding to the majority of the occupying phases is applied.

$f_i^{k\ eq}$ is the equilibrium distribution function, which depends on the local density, the local velocity, and τ_k, which is the relaxation parameter for species k. The equilibrium distribution functions have to verify the mass conservation and the momentum conservation constraints as follows:

$$\begin{aligned} \rho_k &= \sum_i f_i^k = \sum_i f_i^{k\ eq} \qquad (k = \alpha, \beta), \\ \rho u &= \sum_{i,k} f_i^k e_i = \sum_{i,k} f_i^{k\ eq} e_i \qquad (k = \alpha, \beta). \end{aligned} \tag{7}$$

We used the following equilibrium distribution functions:

$$\begin{aligned} f_i^{\alpha\ eq} &= \rho w_i \left[r_i + 3 e_i.u + \frac{9}{2}\left(e_i.u\right)^2 - \frac{3}{2}u^2 \right], \\ f_i^{\beta\ eq} &= \rho w_i \left[1 + 3 e_i.u + \frac{9}{2}\left(e_i.u\right)^2 - \frac{3}{2}u^2 \right], \end{aligned} \tag{8}$$

where w_i is the weighting factor associated with the direction i and r_i allows the conservation of momentum near the interface between the two phases. Indeed, in this region, we observe a mixing of the two species, which can create non-physical constraints, especially when the two species have different densities.

$$r_i = \begin{cases} \dfrac{\rho_\beta}{\rho_\alpha} & i = 0 \\ \dfrac{1}{4}\left(9 - \dfrac{5\rho_\beta}{\rho_\alpha}\right) & i = 1,2...8 \end{cases} \tag{9}$$

The present model is based on the basic concepts of the Gunstensen method and executes the following operations at each time step: 1) streaming, 2) boundary-conditions, 3) collision, 4) body forces, and 5) segregation/recoloring. However, it differs from the Gunstensen method in two ways: the surface tension model and the segregation process are improved.

Instead of using another collision step to apply surface tension at the interface, the present method uses the concept of continuum surface force (CSF) developed by Brackbill et al. [31], applied to the lattice Boltzmann method by Lishchuk [9] and improved by Halliday [32] The surface tension is modeled as a body force s applied directly across the interface according to the following equation:

$$s_i = \frac{3}{2}\kappa\sigma w_i \nabla[VOF] n_i . e_i \tag{10}$$

in which σ is the surface tension, κ is the local curvature of the interface, and VOF is the volume of fluid function defined as

$$VOF(x,t) = \frac{\rho_\alpha(x,t) - \rho_\beta(x,t)}{\rho_\alpha(x,t) + \rho_\beta(x,t)}. \tag{11}$$

This method exercises direct control over surface tension value, models with accuracy the surface tension effect, and is easy to implement.

The second improvement concerns the segregation/recoloring step. The present method uses the diffusion scheme developed by Latva-Kokko [10]. The advantages of this scheme are that it reduces the problem of lattice pinning and keeps the color

distribution symmetric around the color gradient. The post-segregation distribution functions are

$$
\begin{aligned}
f_i^{\alpha} &= \frac{\rho_{\alpha}}{\rho_{\alpha}+\rho_{\beta}} f_i + \delta \frac{\rho_{\alpha}\rho_{\beta}}{\left(\rho_{\alpha}+\rho_{\beta}\right)^2} f_i^{eq\,0} \cos(\varphi) \\
f_i^{\beta} &= \frac{\rho_{\beta}}{\rho_{\alpha}+\rho_{\beta}} f_i - \delta \frac{\rho_{\alpha}\rho_{\beta}}{\left(\rho_{\alpha}+\rho_{\beta}\right)^2} f_i^{eq\,0} \cos(\varphi)
\end{aligned}
\tag{12}
$$

where $f_i^{eq\,0}$ is the zero-velocity equilibrium distribution and δ characterizes the tendency of the fluid to separate. As δ increases, the interface width decreases. If δ is more than one, f_i^k can be negative. However, if δ is kept small enough, the scheme remains stable. For our study, δ equals one.

In the case of a planar and immobile interface, the discontinuity problem at the interface has been investigated by Ginzburg who derived a two-relaxation-time collision operator (TRT) to satisfy continuity at the interface. This TRT operator defines $\tilde{f}_i^k$, the post collision value for the direction i as follows:

$$
\tilde{f}_i^k = f_i^{eq} + \left[1+\lambda_e\right]\left[f_i^{+} - f_i^{eq+}\right] + \left[1+\lambda_o\right]\left[f_i^{-} - f_i^{eq-}\right], \tag{13}
$$

with

$$
\begin{cases}
f_i^{+} = \dfrac{f_i + f_{\bar{i}}}{2} \\
f_i^{-} = \dfrac{f_i - f_{\bar{i}}}{2} \\
f_i^{eq+} = \dfrac{f_i^{eq} + f_{\bar{i}}^{eq}}{2} \\
f_i^{eq-} = \dfrac{f_i^{eq} - f_{\bar{i}}^{eq}}{2}.
\end{cases}
\tag{14}
$$

The continuity and stability conditions are

$$\lambda_o = -8\frac{\lambda_e + 2}{\lambda_e + 8}, \tag{15}$$

$-2 \le \lambda_s < 0 \quad s = (e, o)$, respectively.

The TRT collision operator cannot guaranty continuity at the interface when the two fluids have different densities. Ginzburg explains [33] that for the case of parabolic flow (e.g., Poiseuille flow) the pressure distribution is uniform, which means that the solution for f_i does not depend on the sound speed or the density. Therefore, the tangential velocity $u = \frac{1}{\rho}\sum f_i$ is discontinuous at the interface since ρ is discontinuous.

Interparticle-potential model

We use the same notation that we used for the color-fluid model: f_i^k represents the single-phase distribution function for the fluid k (k=β or k=α) and the evolution of the distribution function for each phase is described as follows.

$$f_i^k(x + e_i, t+1) = f_i^k(x,t) + \Omega_i^k(x,t). \tag{16}$$

In order to include the surface tension and to force the two phases to segregate, Shan and Chen [2, 3] used a modified BGK collision operator Ω_i^k with the following equilibrium distribution functions, which allows the simulation of phases with different densities:

$$f_i^{k\ eq} = n_k w_i \left[r_i + 3e_i.u_k^{eq} + \frac{9}{2}\left(e_i.u_k^{eq}\right)^2 - \frac{3}{2}u_k^{eq2} \right] \tag{17}$$

where

$$
\begin{aligned}
n_k &= \frac{\rho_k}{m_k}, \\
r_0 &= \frac{1}{4}\left(9 - \frac{5}{\rho_{k\,init}}\right), \\
r_i &= \frac{1}{\rho_{k\,init}} \qquad (i = 1, 2, \ldots 8).
\end{aligned}
\tag{18}
$$

The equilibrium distribution functions have to verify the mass conservation and the momentum conservation constraints as follows:

$$
\begin{aligned}
\rho_k &= m_k \sum_i f_i^k \qquad (k = \alpha, \beta), \\
\rho_k u_k &= m_k \sum_i f_i^k e_i \quad (k = \alpha, \beta).
\end{aligned}
\tag{19}
$$

To model the interaction between components, a modified equilibrium velocity is defined as

$$
\rho_k u_k{}^{eq} = \rho_k u' + \tau_k F_k . \tag{20}
$$

u' is determined by the relation

$$
u' = \left(\sum_k \frac{\rho_k u_k}{\tau_k}\right) / \left(\sum_k \frac{\rho_k}{\tau_k}\right). \tag{21}
$$

$F_k(x)$ is the interactive force applied on component k at site x. This force tends to separate phases by pushing k-components into phase k. The interparticle-potential model uses a nearest neighbor interaction force defined as follows:

$$
F_k(x) = -g_{k\bar{k}} \psi_k(x) \sum_k w_k \psi_{\bar{k}}(x + e_k) e_k , \tag{22}
$$

where $\psi_k(x)$ is a function of the local density, and $g_{k\bar{k}}$ is the coupling constant controlling the strength of the interaction and therefore the surface tension.

The density and the macroscopic velocity of the mixture are defined as [3]:

$$\rho = \sum_k \rho_k$$
$$\rho v = \sum_k \rho_k u_k + \frac{1}{2}\sum_k F_k \tag{23}$$

Particle momentum at each site is not conserved due to the interaction force. However, the total momentum of the system is conserved.

In the interparticle-potential model, the interface between two phases is finite but not sharp. The width of the interface is controlled by the coupling constant $g_{k\bar{k}}$ as increasing $g_{k\bar{k}}$ will decrease the width of the interface. However, $g_{k\bar{k}}$ cannot be set too high, or the simulation will blow up. Figure 2 shows the characteristic of an interface between two phases α and β with $\frac{\nu_\alpha}{\nu_\beta} = 1$, $\frac{\rho_\alpha}{\rho_\beta} = 2$, and $g_{k\bar{k}}$ equals 1.0. We can observe in this figure that phase k (α or β) has a constant non-zero density in the $\bar{k}$-layer (β or α), so the two phases are not exactly immiscible. However, we can consider the two phases immiscible because the two layers are distinct and the interface is finite (the width of the interface equals approximately five lattice lengths in this particular case).

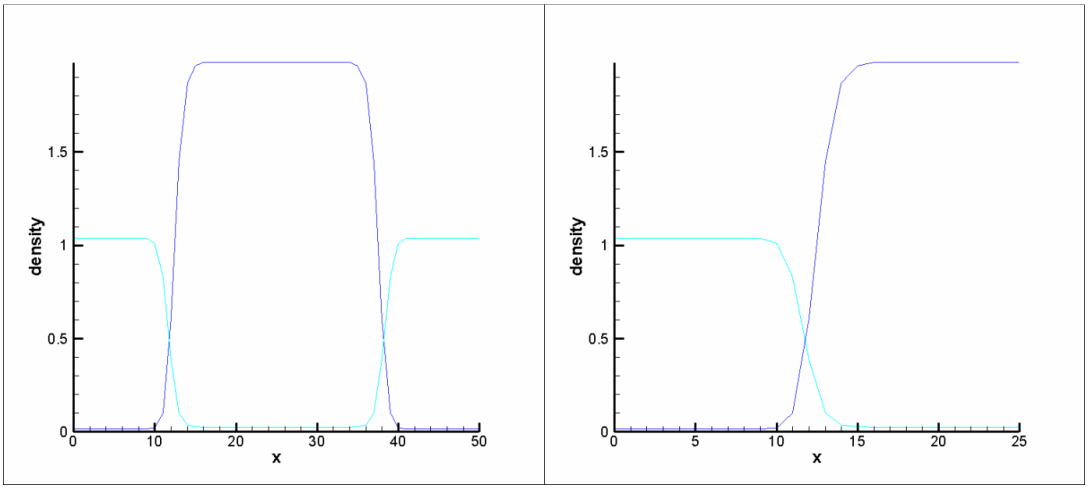

Figure 2: Density distribution across the channel

It is important to note that the following characteristics of the flow change as the simulation continues, until a steady state is reached: the position of the interface, the mean viscosity in each layer, and the mean density in each layer. The interface moves because of the interaction forces applied at the interface; the mean density and viscosity in each layer differ from the initial density and viscosity because the two phases are not exactly immiscible. These characteristics are determined at the end of the simulation as follows:

$$x \in \text{interface} \Leftrightarrow \rho_{\mathrm{k}}(x) = \rho_{\bar{\mathrm{k}}}(x),$$

$$\begin{cases} \nu_\alpha = \left[\left(\dfrac{1}{N_\alpha \left(\rho_k + \rho_{\bar{k}} \right)} \displaystyle\sum_{\alpha - layer} \rho_k \tau_k + \rho_{\bar{k}} \tau_{\bar{k}} \right) - \dfrac{1}{2} \right] \dfrac{1}{3}, \\ \rho_k = \dfrac{1}{N_\alpha \left(\rho_k + \rho_{\bar{k}} \right)} \displaystyle\sum_{\alpha - layer} \rho_k + \rho_{\bar{k}}, \end{cases} \tag{24}$$

$$\begin{cases} \nu_\beta = \left[\left(\dfrac{1}{N_\beta \left(\rho_k + \rho_{\bar{k}} \right)} \displaystyle\sum_{\beta - layer} \rho_k \tau_k + \rho_{\bar{k}} \tau_{\bar{k}} \right) - \dfrac{1}{2} \right] \dfrac{1}{3}, \\ \rho_\beta = \dfrac{1}{N_\beta \left(\rho_k + \rho_{\bar{k}} \right)} \displaystyle\sum_{\beta - layer} \rho_k + \rho_{\bar{k}}, \end{cases} \tag{25}$$

where N_α is the number of nodes in the α–layer and N_β is the number of nodes in the β –layer.

Free-energy model

We implemented two free-energy-based methods presented here in detail. In a first part, we describe the original free-energy method developed by Orlandini et al. [19] and Swift et al. [4], and in a second part, we describe the free-energy method for large density ratios developed by Zheng et al. [23].

Original free-energy model

The model proposed by Orlandini et al. [19] and Swift et al. [4] considers the total density and the density difference instead of the density of the each fluids, contrary to the color-fluid method and the interparticle-potential method .

We use the following free energy functional, which is based on the Ginzburg-Landau expression of the free-energy density [34]

$$\mathbf{F} = \int \left\{ \frac{1}{3} n \ln(n) + \frac{a}{2}\varphi^2 + \frac{b}{4}\varphi^4 + \frac{\kappa}{2}\left(\nabla\varphi\right)^2 \right\} dr \quad , \tag{26}$$

where n is the total (number) density $n_\alpha + n_\beta$ and φ is the (number) density difference between the two fluids $n_\alpha - n_\beta$ where n_α and n_β are the (number) densities of the two fluids.

The chemical potential difference between the two fluids $\Delta\mu$ and the pressure tensor P_{kl} are given by

. $$\Delta\mu = \frac{\partial F}{\partial \varphi} = a\varphi + b\varphi^3 - \kappa\left(\nabla\varphi\right)^2 \tag{27}$$

$$P_{kl} = p_0\delta_{kl} + \kappa\partial_k\varphi\partial_l\varphi \tag{28}$$

respectively, where p_0 is the diagonal coefficient and can by expressed as

$$p_0 = n\frac{\partial F}{\partial n} + \varphi\frac{\partial F}{\partial \varphi} - \frac{1}{3}n\ln(n) + \frac{a}{2}\varphi^2 + \frac{b}{4}\varphi^4 + \frac{\kappa}{2}\left(\nabla\varphi\right)^2$$

$$p_0 = \frac{1}{3}n + \frac{a}{2}\varphi^2 + \frac{3b}{4}\varphi^4 - \frac{\kappa}{2}\left(\nabla\varphi\right)^2 - \kappa\left(\nabla^2\varphi\right) \tag{29}$$

To describe the two phases, we use two sets of distribution functions $f_i(x,t)$ and $g_i(x,t)$, which evolve as follows

$$f_i(x+e_i,t+1)=f_i(x,t)-\frac{1}{\tau}\left[f_i-f_i^{eq}\right]$$

$$g_i(x+e_i,t+1)=g_i(x,t)-\frac{1}{\tau_\varphi}\left[g_i-g_i^{eq}\right] \tag{30}$$

The equilibrium distribution functions have to verify the volume conservation and the momentum conservation constraints as follows:

$$\begin{cases} n=\sum_i f_i \\ \varphi=\sum_i g_i \\ nu=\sum_i f_i\, e_i \end{cases} \tag{31}$$

The following equilibrium distribution functions can be used to implement this method with a 2D9Q lattice [34].

$$\begin{aligned} f_0^{eq} &= A_0+C_0u^2 \\ f_i^{eq} &= n\left[A_I+B_I\frac{e_i.u}{c^2}+C_I\frac{\left(e_i.u\right)^2}{c^4}+D_I\frac{\left(u.u\right)}{c^2}\right]+G_{I\,kl}e_{ik}.e_{il} \qquad i=1,2,3,4 \\ f_i^{eq} &= n\left[A_{II}+B_{II}\frac{e_i.u}{c^2}+C_{II}\frac{\left(e_i.u\right)^2}{c^4}+D_{II}\frac{\left(u.u\right)}{c^2}\right]+G_{II\,kl}e_{ik}.e_{il} \quad i=5,6,7,8 \end{aligned} \tag{32}$$

where

$$\begin{aligned} &A_{II}=\frac{P_{kl}\delta_{kl}}{24} \qquad A_I=4A_{II} \qquad A_0=n-20A_{II} \\ &B_{II}=\frac{n}{12c^2} \qquad B_I=4B_{II} \\ &C_{II}=-\frac{n}{24c^2} \qquad C_I=4C_{II} \qquad C_0=\frac{2n}{3c^2} \\ &D_{II}=\frac{n}{9c^4} \qquad D_I=4D_{II} \\ &G_{II\,kl}=\frac{P_{kl}-0.5P_{\sigma\sigma}\delta_{kl}}{8c^2} \qquad G_{I\,kl}=4G_{II\,kl} \end{aligned} \tag{33}$$

The coefficients for g_i are obtained by substituting P_{kl} with $\Gamma\Delta\mu\delta_{kl}$ and n with φ.

To simulate two phases with two different viscosities τ has to be a function of $\Delta n / n$ as presented by Langaas [35]. Langaas used the model of "ideal" mixture viscosity of a binary mixture developed by Arrhenius. The fluid viscosity can be expressed as

$$\nu = \nu_\alpha^{\frac{n+\Delta n}{2n}} \nu_\beta^{\frac{n-\Delta n}{2n}} . \tag{34}$$

It follows that

$$\tau = 3\nu_\alpha^{\frac{n+\Delta n}{2n}} \nu_\beta^{\frac{n-\Delta n}{2n}} + \frac{1}{2} . \tag{35}$$

Free-energy method for large density ratios

Zheng et al. [23] developed a method based on the free energy approach for large density ratios up to 1000.

n and ϕ (order parameter) are the two macroscopic variables used to describe a flow with two phases having different densities, and are defined as follows

$$n = \frac{\rho_\alpha + \rho_\beta}{2},$$

$$\phi = \frac{\rho_\alpha - \rho_\beta}{2}, \tag{36}$$

where ρ_α and ρ_β, are the densities of the two fluids considered.

Zheng used the following lattice Boltzmann equation

$$g_i(x+e_i,t+1) = g_i(x,t) + (1-q)\left[g_i(x+e_i,t) - g_i(x,t)\right] - \frac{1}{\tau_\phi}\left[g_i - g_i^{eq}\right],$$

$$f_i(x+e_i,t+1) = f_i(x,t) - \frac{1}{\tau_n}\left[f_i - f_i^{eq}\right] + \left(1 - \frac{1}{2\tau}\right) 3w_i\left[\left(e_i - u\right) + 3\left(e_i.u\right)e_i\right]\left(\mu_\phi \vec{\nabla}\phi + F_b\right) \tag{37}$$

F_b is a body force and μ_ϕ is the chemical potential and is defined as

$$\mu_\phi = A\left(4\phi^3 - 4\phi^{*2}\phi\right) - \kappa\nabla^2\phi, \tag{38}$$

Where A controls the interaction energy between the two phases and κ is a constant related to the surface tension.

In order to recover the Cahn-Hilliard equation, which model interface capturing, q is set to be

$$q = \frac{1}{\tau_\phi + 0.5}. \tag{39}$$

The distribution functions satisfy the conservation laws

$$\begin{cases} \phi = \sum_i g_i = \sum_i g_i^{eq} \\ \dfrac{\phi}{q}u \equiv \sum_i g_i e_i \\ \Gamma\mu_\phi\delta_{kl} = \sum_i g_i^{eq} e_{ik}.e_{il} \end{cases} \tag{40}$$

$$\begin{cases} n = \sum_i f_i = \sum_i f_i^{eq} \\ u = \dfrac{\sum_i f_i e_i + \frac{1}{2}\left(\mu_\phi\vec{\nabla}\phi + F_b\right)}{n} \\ \left(\phi\mu_\phi + {c_s}^2 n\right)\delta_{kl} + nu_k u_l = \sum_i f_i^{eq} e_{ik}.e_{il} \end{cases} \tag{41}$$

The equilibrium distribution functions $g^{eq}(x,t)$ and $f^{eq}(x,t)$ are defined as

$$g_i^{eq} = A_i + B_i\phi + C_i\phi e_i.u,$$

$$f_i^{k\,eq} = w_i D_i + w_i n\left[3e_i.u + \frac{9}{2}\left(e_i.u\right)^2 - \frac{3}{2}u^2\right] \tag{42}$$

To describe $g(x,t)$ and $f(x,t)$, Zheng used a D2Q5 and a D2Q9 lattices, respectively. Based on these discretizations, the coefficients are

$$\begin{aligned} &A_0 = -2\Gamma\mu_\phi \qquad A_i = \frac{1}{2}\Gamma\mu_\phi \qquad (i \neq 0) \\ &B_0 = 1 \qquad B_i = 0 \qquad (i \neq 0) \\ &C_i = \frac{1}{2q} \\ &D_0 = \frac{9}{4}n - \frac{15\left(\phi\mu_\phi + \frac{1}{2}n\right)}{4} \qquad D_i = 3\left(\phi\mu_\phi + \frac{1}{2}n\right) \qquad (i \neq 0) \end{aligned} \tag{43}$$

where Γ controls the mobility.

The thickness of the interface W and the surface tension σ can be evaluated by $W = \frac{\sqrt{2\kappa / A}}{\phi^*}$ and $\sigma = \frac{4\sqrt{2\kappa A}}{3}\phi^{*3}$, where ϕ^* is the expected order parameter $\phi^* = \frac{\rho_\alpha - \rho_\beta}{2}$.

Mean-field theory model

He et al. [5, 25] proposed a lattice-Boltzmann model for two-phase flow, valid in the nearly incompressible limit. In this model, phase segregation and surface tension are modeled by incorporating molecular interaction forces, which are approximated by the mean-field theory model.

The model developed by He et al. uses two distributions functions: $\tilde{g}_i(x,t)$ describes the evolution of the pressure p and $\tilde{f}_i(x,t)$ describes the evolution of the index function ϕ which is used to track the interface. These distribution functions satisfy the following discrete evolution equations [25]

$$\tilde{f}_i(x+e_i,t+1)=\tilde{f}_i(x,t)-\frac{1}{\tau}\left[\tilde{f}_i-\tilde{f}_i^{eq}\right]-\frac{2\tau-1}{2\tau RT}\left(e_i-u\right)\nabla\psi(\phi)\Gamma_1(u)$$

$$\tilde{g}_i(x+e_i,t+1)=\tilde{g}_i(x,t)-\frac{1}{\tau}\left[\tilde{g}_i-\tilde{g}_i^{eq}\right]+\frac{2\tau-1}{2\tau}\left(e_i-u\right)\left[\Gamma_1(u)\left(F_s+G\right)-\left(\Gamma_1(u)-\Gamma_1(0)\right)\nabla\psi(\phi)\right] \tag{44}$$

where

$$\Gamma_1(u)=w_i\left[1+\frac{3e_i.u}{c^2}+\frac{9\left(e_i.u\right)^2}{2c^4}-\frac{3\left(u.u\right)}{2c^2}\right]. \tag{45}$$

R is the gas constant, T is the bulk temperature, G is the gravitational force, and F_s is the surface tension force defined by

. $$F_s=\kappa\phi\nabla\nabla^2\phi \tag{46}$$

where κ controls the strength of the surface tension

The equilibrium functions $\tilde{f}_i^{eq}$ and $\tilde{g}_i^{eq}$ are defined as [14]

$$\tilde{f}_i^{eq}=w_i\phi\left[1+\frac{3e_i.u}{c^2}+\frac{9\left(e_i.u\right)^2}{2c^4}-\frac{3\left(u.u\right)}{2c^2}\right],$$

$$\tilde{g}_i^{eq}=w_i\left[p+\rho RT\left(\frac{3e_i.u}{c^2}+\frac{9\left(e_i.u\right)^2}{2c^4}-\frac{3\left(u.u\right)}{2c^2}\right)\right]. \tag{47}$$

In this study, the function $\psi\left(\phi\right)$, which is directly related to phase separation, has the form of the Carnahan-Starling equation of state for a non ideal gas

$$\psi\left(\phi\right)=\phi^2RT\frac{4-2\phi}{\left(1-\phi\right)^3}-a\phi^2 \tag{48}$$

where a determines the strength of the molecular interactions. Figure 3 shows the curve of the function $\psi\left(\phi\right)+\phi RT$, which has two stable roots ϕ_h and ϕ_l and one unstable root $\left(d(\psi(\phi))+\phi RT\right)/d\phi<0$. This unstable range of ϕ causes phase separation by

pushing the index function toward ϕ_α or ϕ_β. In this study, we use $a = 12RT$ and $\psi(\phi) + \phi RT = 0.01$, which give $\phi_\alpha = 0.260$ and $\phi_\beta = 0.045$.

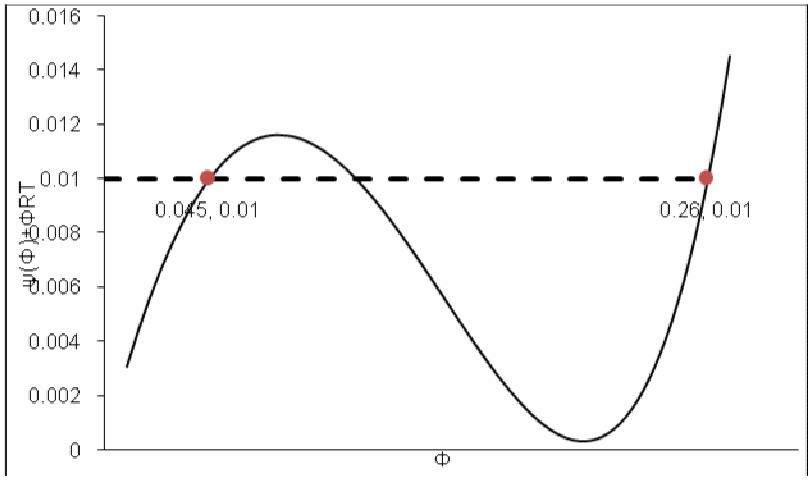

Figure 3: function $\psi(\phi) + \phi RT$

The macroscopic variables are evaluated as follows

$$\begin{aligned}
\phi &= \sum_i \tilde{f}_i, \\
p &= \sum_i \tilde{g}_i - \frac{1}{2} u.\nabla \psi(\rho), \\
\rho RTu &= \sum_i e_i \tilde{g}_i - \frac{RT}{2}(F_s + G), \\
\rho(\phi) &= \rho_l + \frac{\phi - \phi_\beta}{\phi_\alpha - \phi_\beta}(\rho_\alpha - \rho_\beta), \\
u(\phi) &= u_l + \frac{\phi - \phi_\beta}{\phi_\alpha - \phi_\beta}(u_\alpha - u_\beta),
\end{aligned} \tag{49}$$

where ρ_α and ρ_β are the densities of the light fluid and the heavy fluid, respectively, and u_α and u_β are the kinematic viscosities of the light fluid and the heavy fluid, respectively.

CHAPTER 3

POISEUILLE TWO-PHASE FLOW AND CONTINUITY ISSUE AT THE INTERFACE

Test case: two-phase Poiseuille flow

We consider a two-phase Poiseuille flow in order to investigate the accuracy of lattice-Boltzmann two-phase flow models at the interface of two fluids. These models can lead to a discontinuity in the tangential velocity at the interface. Our goal is to assess this error by comparing the analytical solution with the results that we obtained with the different methods. We also investigate discrepancies that are not located at the interface. We show the results by superposing the analytical solution represented by a green line (-) and the result of the simulation represented by red squares (□). The following figure introduces the notations.

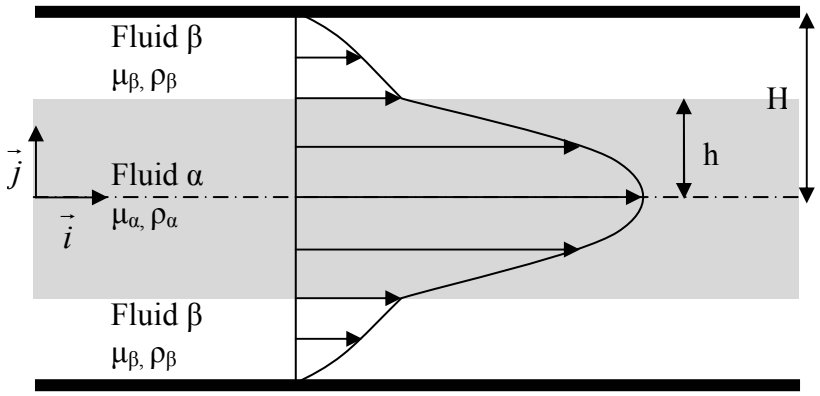

Figure 4: Channel – Poiseuille flow

H is the half width of the channel, μ_α and μ_β are the viscosities of the light fluid and the heavy fluid, respectively, ρ_α and ρ_β are the densities of the light fluid and the heavy

fluid, respectively, and the flow is driven by a small force field f, which acts like a pressure gradient. The flows simulated are small, and no instabilities occur at the interface of the two phases. In this case, the velocity field is given by these equations:

$$u_\alpha = -A_\alpha y^2 + D_\alpha \qquad \text{for} \qquad 0 \le y \le h,$$

$$u_\beta = -A_\beta y^2 + C_\beta + D_\beta \qquad \text{for} \qquad h \le y \le H, \tag{10}$$

where

$$A_\alpha = \frac{f}{2\nu_\alpha} \qquad A_\beta = \frac{f}{2\nu_\beta},$$

$$C_\beta = 2\left(A_\beta - \frac{\mu_\alpha}{\mu_\beta} A_\alpha \right) h \tag{51}$$

$$D_\beta = A_\beta H^2 - C_\beta H, \quad D_\alpha = \left(A_\alpha - A_\beta \right) h^2 + C_\beta h + D_\beta$$

To ensure that the analytical solution used as reference is correct, we need an accurate estimate of h. One issue is that the interface is located between two rows of grid nodes and not on one row of grid nodes. Another issue is the fact that the interface can move during the simulation because of interaction forces.

Results obtained with the color-fluid model

With the BGK collision operator, we considered the following cases:

Table 1: simulations with the color-fluid model (BGK collision operator)

Simulation#	τα	τβ	να	νβ	ρα/ρβ	να/νβ	force
1	1	1	0.1666	0.1666	1	1	0.0001
2	1.5	1	0.3333	0.1666	1	2	0.0001
3	5.5	1	1.6667	0.1666	1	10	0.0001
4	50.5	1	16.667	0.1666	1	100	0.0001
5	1	1	0.1666	0.1666	2	1	0.0001
6	1	1	0.1666	0.1666	10	1	0.0001

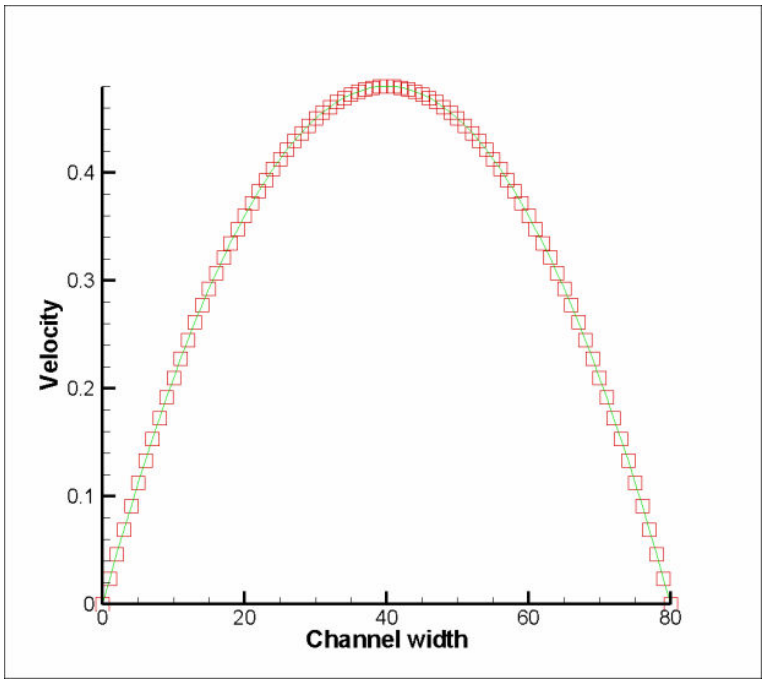

Figure 5: Velocity profile - simulation #1 - color fluid model - BGK collision operator

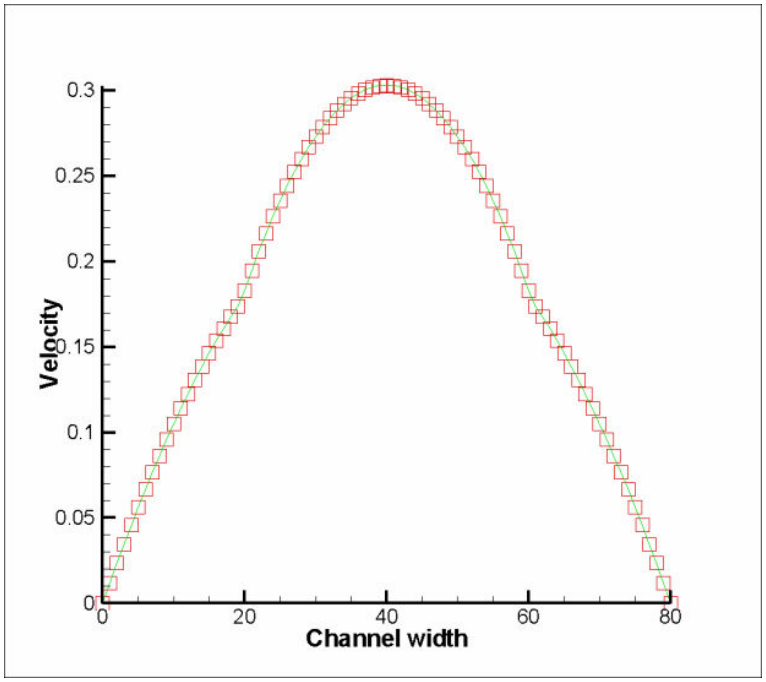

Figure 6: Velocity profile - simulation #2 - color fluid model - BGK collision operator

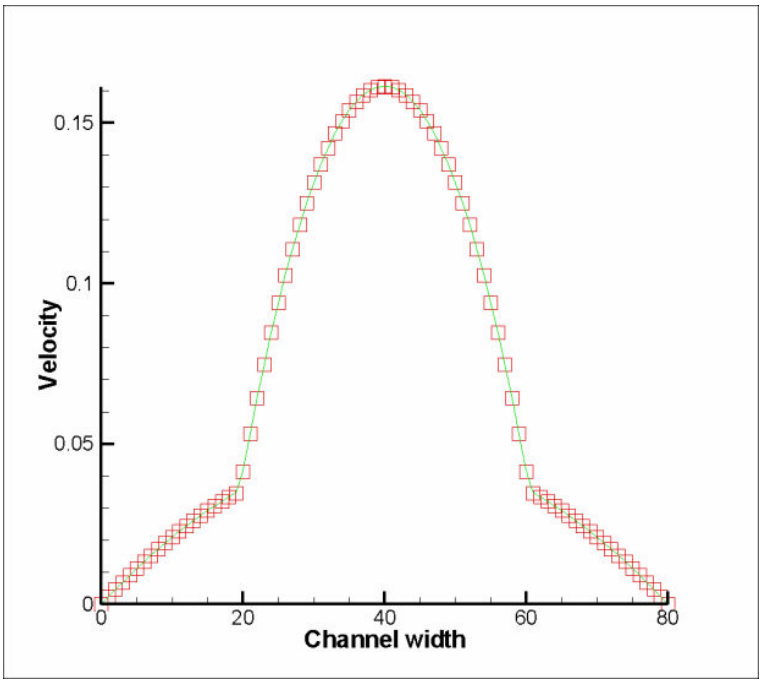

Figure 7: Velocity profile - simulation #3 - color fluid model - BGK collision operator

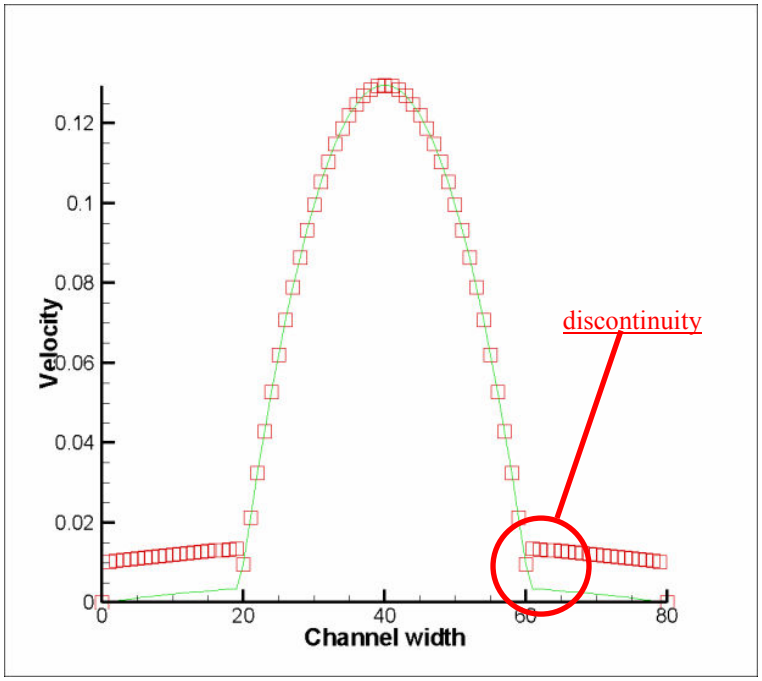

Figure 8: Velocity profile - simulation #4 - color fluid model - BGK collision operator

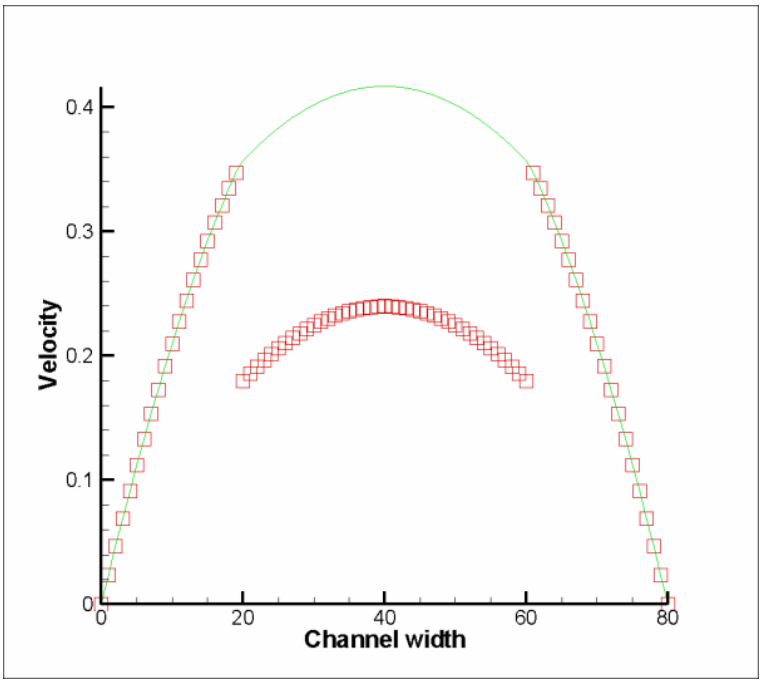

Figure 9: Velocity profile - simulation #5 - color fluid model - BGK collision operator

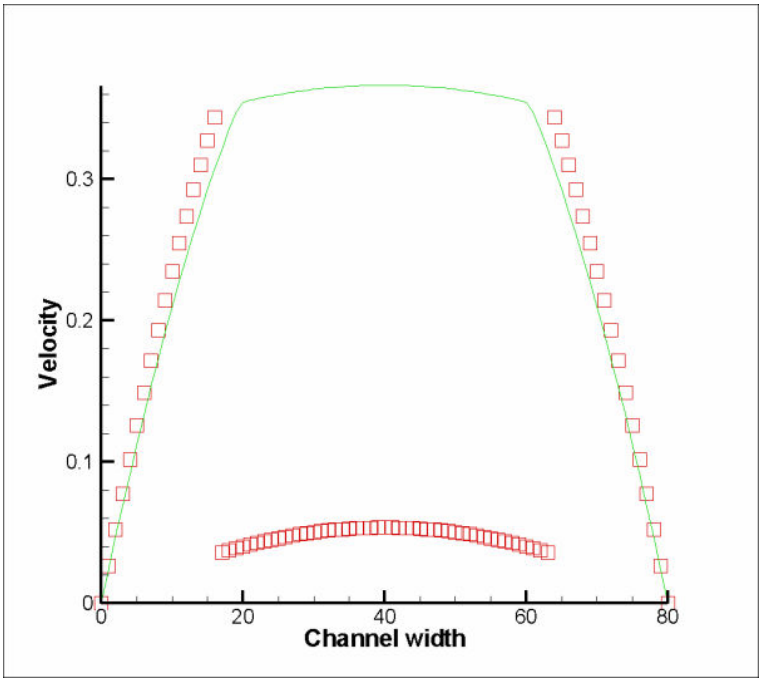

Figure 10: Velocity profile - simulation #6 - color fluid model - BGK collision operator

with the TRT collision operator, we considered the following cases:

Table 2: simulations with the TRT collision operator

Simulation	-λeα	-λeβ	να	νβ	-λoα	-λoβ	$\frac{\rho_\alpha}{\rho_\beta}$	$\frac{\nu_\alpha}{\nu_\beta}$	force
1	1	1	0.1666	0.1666	1.1428571	1.1428571	1	1	0.0001
2	0.6666699	1	0.3333	0.1666	1.4545426	1.1428571	1	2	0.0001
3	0.1818174	1	1.6667	0.1666	1.8604658	1.1428571	1	10	0.0001
4	0.0198020	1	16.667	0.1666	1.9851117	1.1428571	1	100	0.0001
5	1	1	0.1666	0.1666	1.1428571	1.1428571	2	1	0.0001
6	1	1	0.1666	0.1666	1.1428571	1.1428571	10	1	0.0001

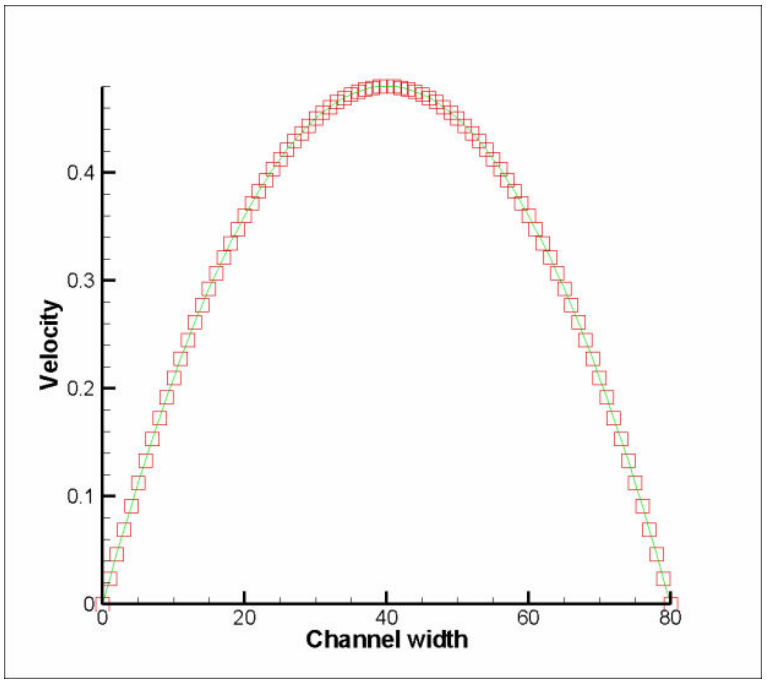

Figure 11: Velocity profile - simulation #1 - color fluid model - TRT collision operator

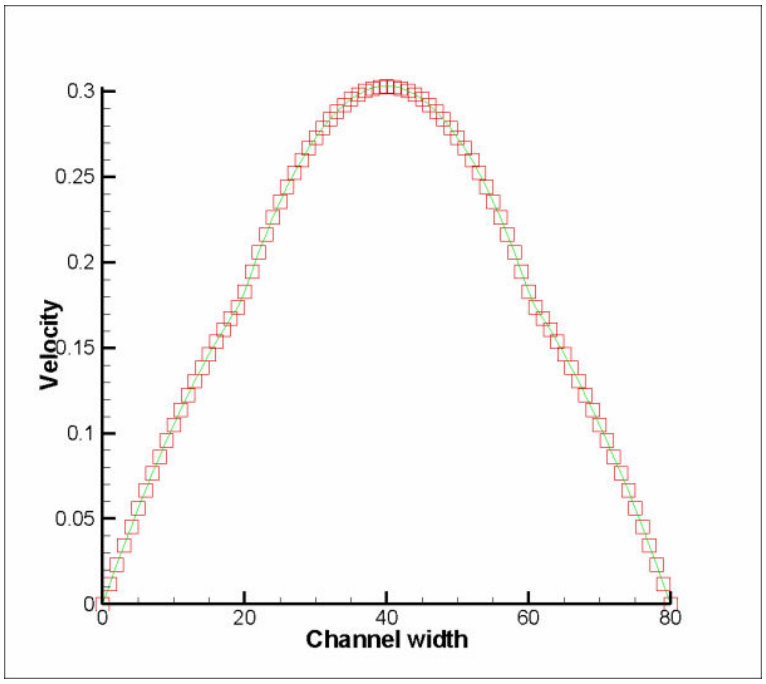

Figure 12: Velocity profile - simulation #2 - color fluid model - TRT collision operator

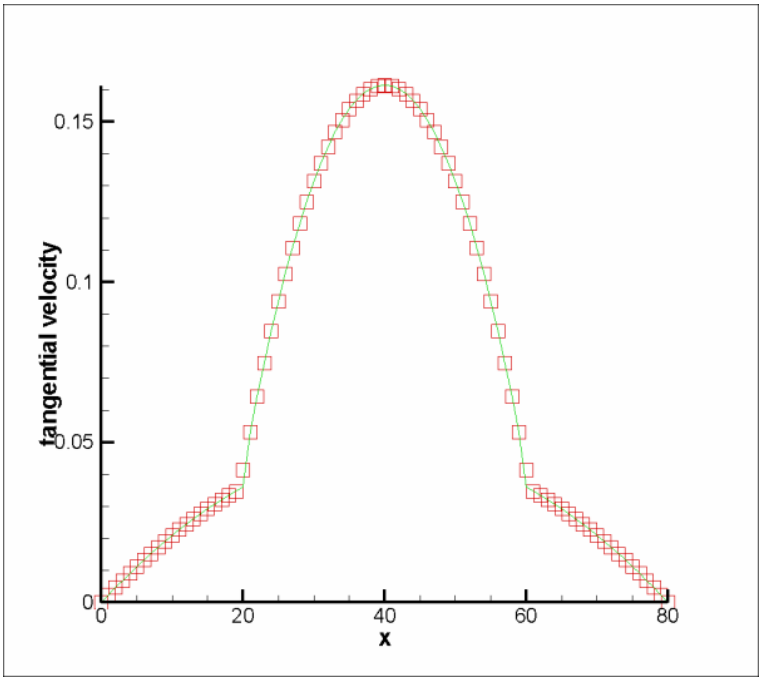

Figure 13: Velocity profile - simulation #3 - color fluid model - TRT collision operator

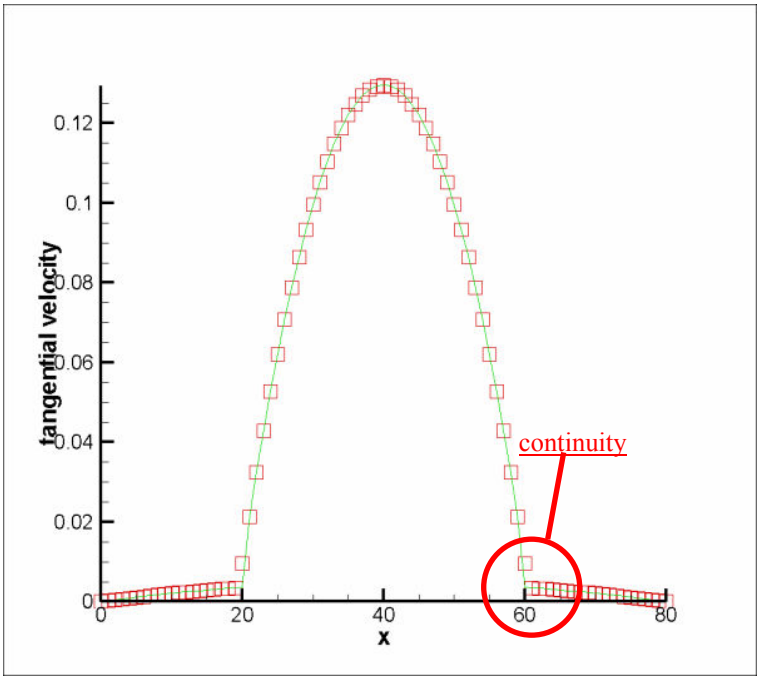

Figure 14: Velocity profile - simulation #4 - color fluid model - TRT collision operator

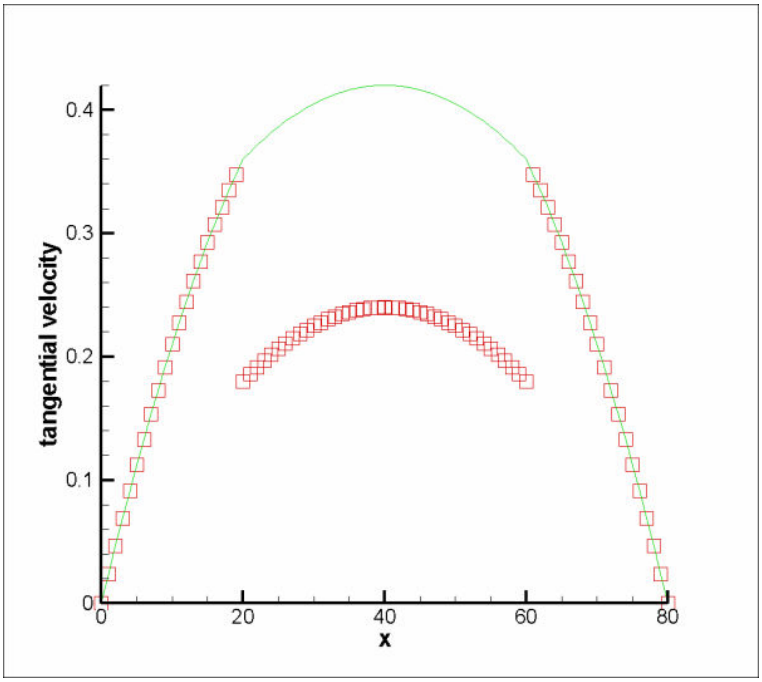

Figure 15: Velocity profile - simulation #5 - color fluid model - TRT collision operator

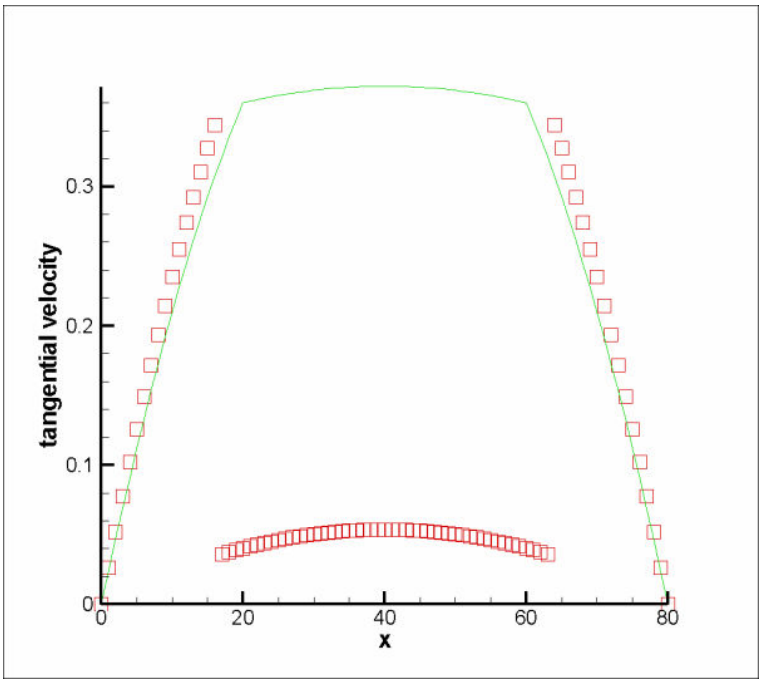

Figure 16: Velocity profile - simulation #6 - color fluid model - TRT collision operator

With the BGK collision operator, the results show a discontinuity of the tangential velocity (error = 286%) if the viscosity ratio is too high (case#4 M = 100). The discontinuity increases as the viscosity ratio increases. For lower viscosity ratios (case#2 and case#3), the main discrepancy is not located at the interface but close to the wall where the error is at a maximum. For case #2, this maximum error is lower than 0.7% so the results show good agreement with the analytical solution. For case#3 the maximum error reaches 40.0%, which deteriorates the accuracy of the results in the outer layer. However, the results of the simulation for case#3 match the analytical solution with an error less than 5% over 80% of the width of the channel. The following table sums up the results when the two fluids have diferent viscosities.

Table 3: results with color-fluid model (BGK collision operator) - different viscosities

case#	average error (%)	maximum error (%)	error at the interface (%)
1	0.1019	0.8439	0.0575
2	0.0714	0.6329	0.0341
3	3.6914	39.4515	0.0784

We observe a large discontinuity when the two fluids have different densities and this discontinuity increases as the density ratio increases (case#5 and case#6).

The TRT model maintains the interface continuity conditions at the interface, even for large viscosity ratios (error = 1.45%). However, the continuity of the tangential velocity is not satisfied if the two fluids have different densities. For small viscosity ratios, the BGK model and the TRT model yield similar results. With both models, the discontinuity is the same in the case of fluids with different densities.

As mentioned earlier, the discontinuity caused by a density difference is inevitable because the pressure distribution is uniform for the case of Poiseuille flow. Since the pressure distribution is uniform, the solution for f_i does not depend on the sound speed or the density and the tangential velocity $u = \frac{1}{\rho}\sum f_i e_i$ undergoes a jump at the interface. By dividing $\sum f_i e_i$ by ρ, the simulation creates a discontinuity proportional to ρ_α / ρ_β therefore the magnitude of the velocity in the inner layer is incorrect. However, the slope of the velocity profile in this inner layer is accurate (maximum error = 0.01%). Hence, we can build a correct velocity profile by adding $\frac{\rho_\beta}{\rho_\alpha} V_{\text{interf}}$ to the velocity in the inner layer, where V_{interf} is defined as the velocity on the

outer side of the interface. This corrected-velocity profile matches the analytical solution with an error less than 1.5%.

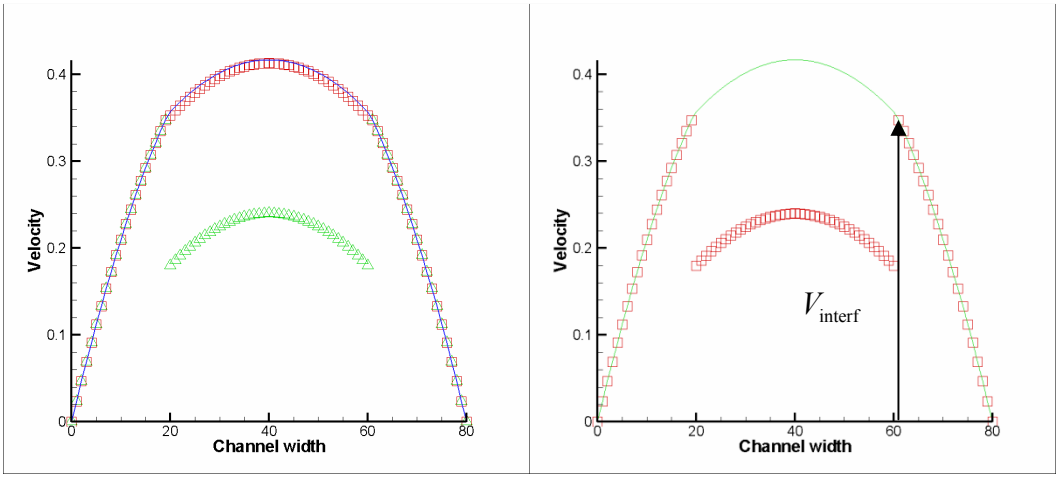

Figure 17: corrected velocity - color-fluid model - density difference

Results obtained with the Interparticle-potential model

We simulated the following cases:

Table 4: simulations with the interparticle-potentials model

Simulation	ρα	ρβ	τα	τβ	να/νβ initial	να/νβ real	ρα/ρβ	interaction constant	force
1	1	1	1	1	1	1	1	1.8	0.0001
2	1	1	2	1	3	1.7192	1	1.8	0.0001
3	1	1	3	0.7	12.5	2.8241	1	1.8	0.0001
4	2	1	1	1	1	1	2	1	0.0001
5	5	1	1	1	1	1	5	0.3	0.0001

The following figures show the density profile across the channel and the comparison between the results of the simulation and the analytical solution for each case.

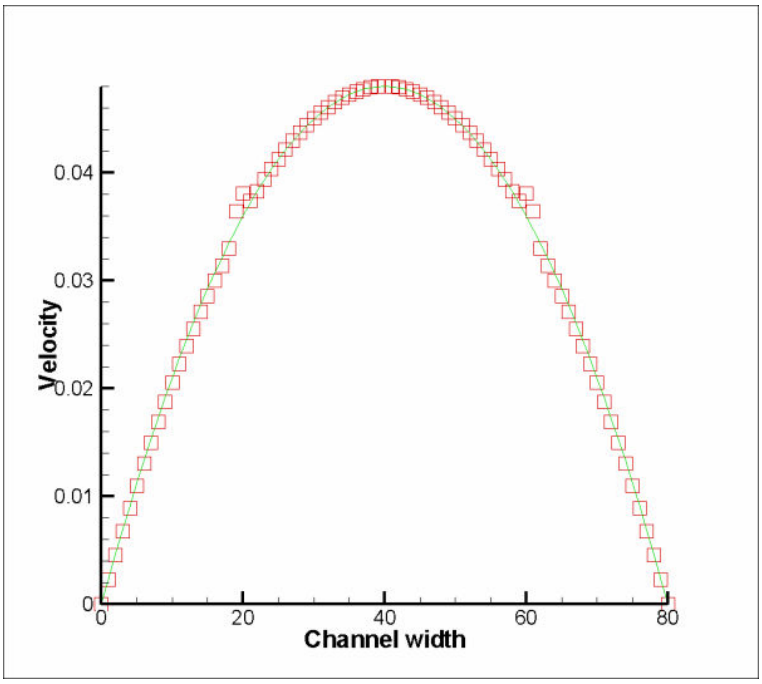

Figure 18: Velocity profile - simulation #1 – interparticle-potentials model

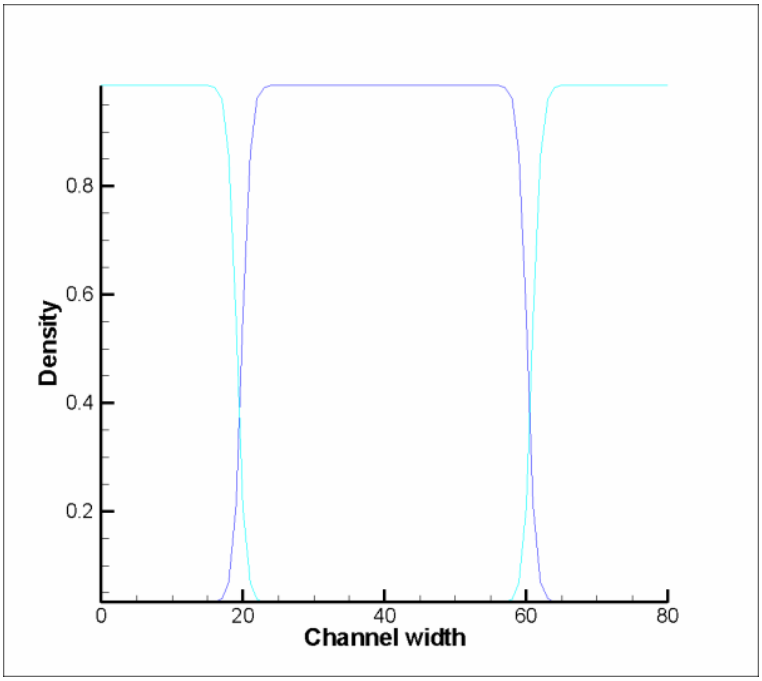

Figure 19: Density profile - simulation #1 – interparticle-potentials model

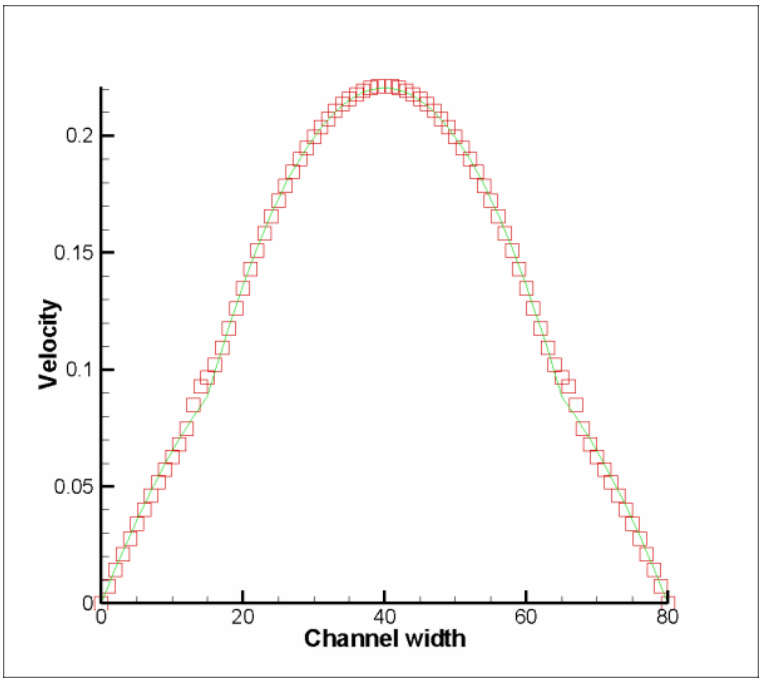

Figure 20: Velocity profile - simulation #2 – interparticle-potentials model

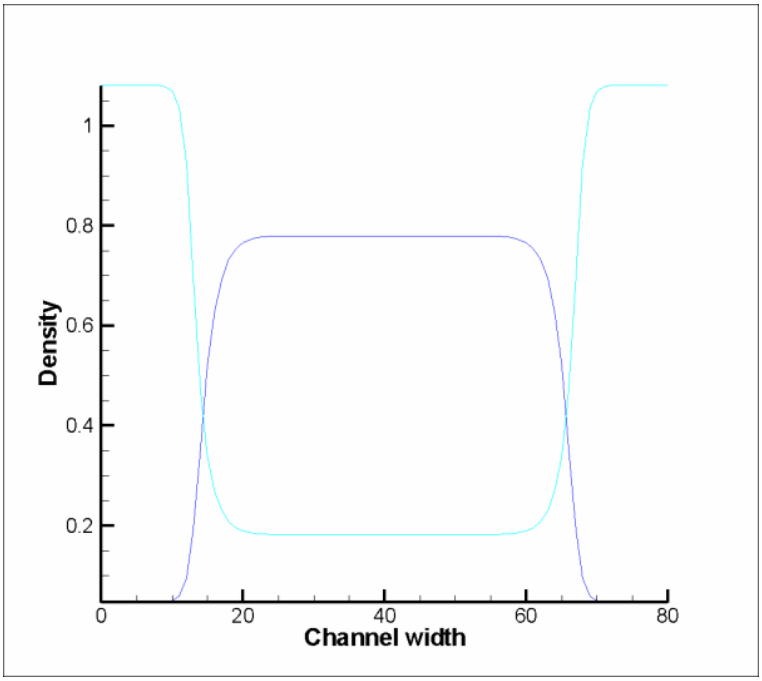

Figure 21: Density profile - simulation #2 – interparticle-potentials model

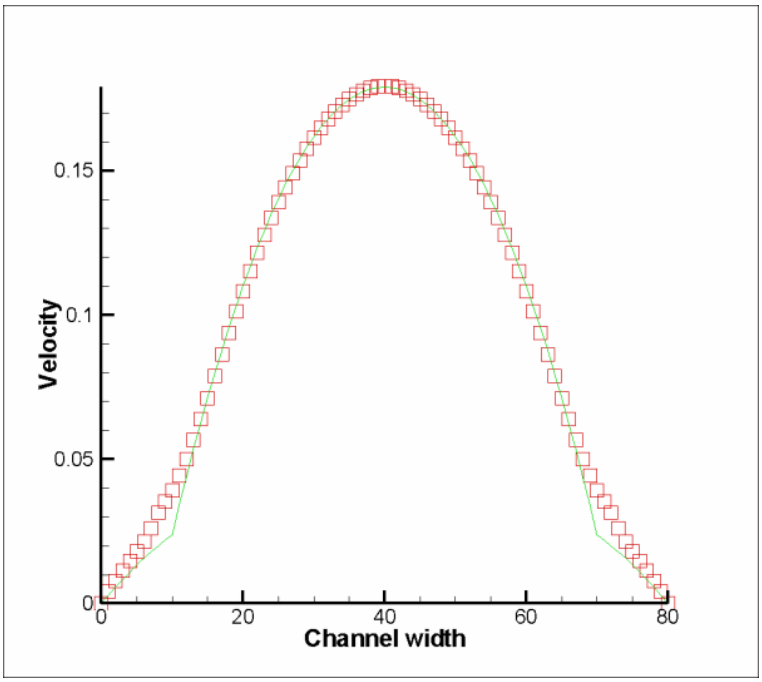

Figure 22: Velocity profile - simulation #3 – interparticle-potentials model

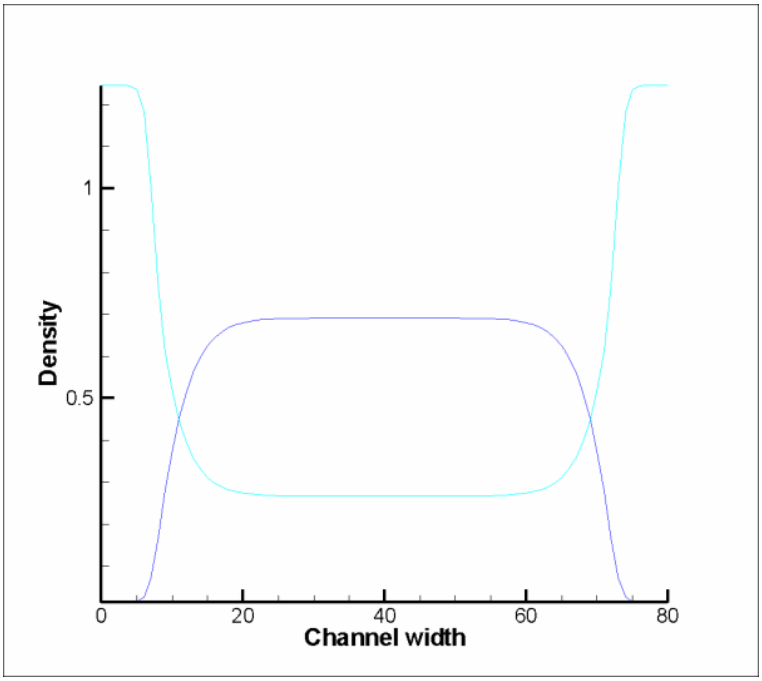

Figure 23: Density profile - simulation #3 – interparticle-potentials model

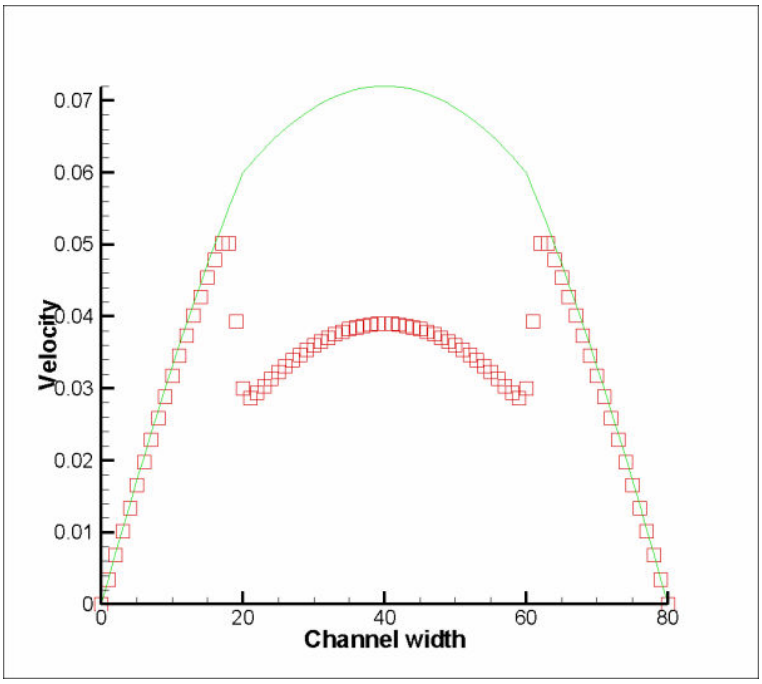

Figure 24: Velocity profile - simulation #4 – interparticle-potentials model

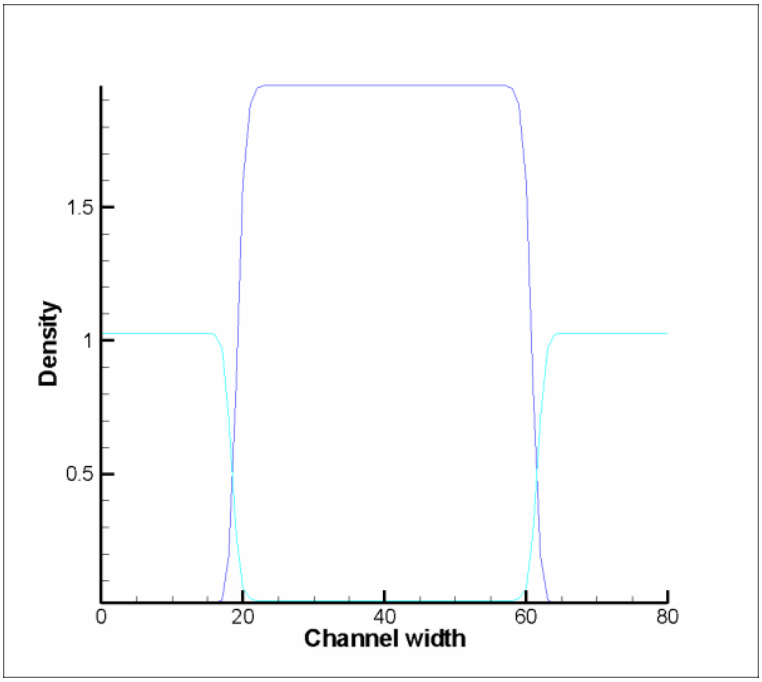

Figure 25: Density profile - simulation #4 – interparticle-potentials model

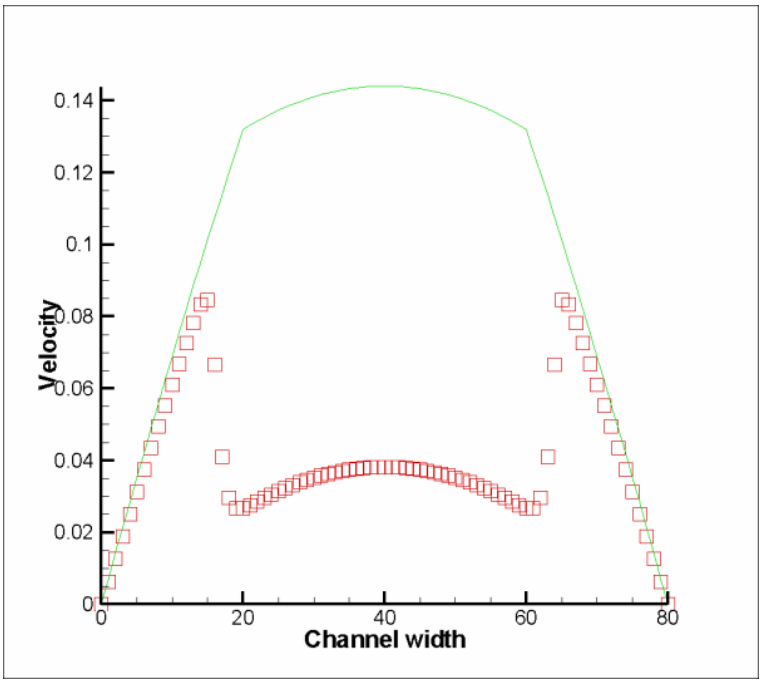

Figure 26: Velocity profile - simulation #5 – interparticle-potentials model

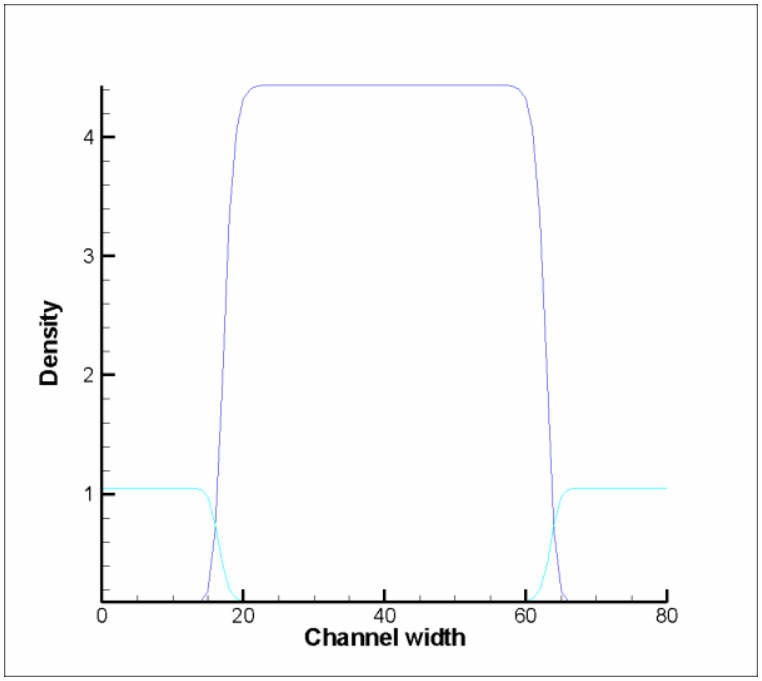

Figure 27: Density profile - simulation #5 – interparticle-potentials model

Even though the two phases have the same density and the same viscosity (case#1), we observe a discontinuity at the interface (error = 6%). Far from the interface, the simulation matches the analytical solution with good accuracy. In the central layer, the error is less than 0.12% and in the side layers, the error is less than 2.4%.

When the two phases have the same density but different viscosities, the immiscibility assumption is no longer valid since we observe a lot of mixing, especially in the inner layer (case #2 and case #3). Even though the two phases are not strictly immiscible, we observe two distinct layers with properties different from the initial conditions (density, viscosity, and location of the interface). For example, in case #2, we started with two phases α and β with $\nu_\alpha = 0.5\text{m}^2.\text{s}^{-1}$ and $\nu_\beta = 0.1666675\text{m}^2.\text{s}^{-1}$ respectively and we ended up with two phases α' and β' with $\nu_{\alpha'} = 0.406497\text{m}^2.\text{s}^{-1}$ and $\nu_{\beta'} = 0.236449\text{m}^2.\text{s}^{-1}$ respectively. We use $\nu_{\alpha'}$ and $\nu_{\beta'}$ to build the analytical solution except for the viscosity ratio M, which has to be evaluated with the original viscosities because the collision operator uses the original values of τ_k. For case#2, the results match with accuracy the analytical solution: the error in the central layer and side layers is less than 1% and 4.4% respectively. However, for case#3, the results give a good order of magnitude but do not match with accuracy the analytical solution. Indeed, the error is less than 2% in the central layer, but in the side layers, the error can be as high as 44%. For both cases, we observe the biggest discrepancy at the interface (case#2 error = 10.2%, case#3 error = 65.1%). The following table sums up the results when the two fluids have diferent viscosities.

Table 5: results with interparticle-potential model - different viscosities

case#	average error	maximum error	error at the interface
1	1.2717	5.8912	5.8912
2	2.0462	10.2037	10.2037
3	12.8314	65.1442	65.1442

If the two phases have different densities, we observe a large discontinuity at the interface. This discontinuity increases as the density ratio increases. The comments made for the color-fluid model for the case of two fluids with different densities apply to the interparticle-potential model as well.

Results obtained with the original free energy model

We simulated the following cases using the original free-energy model:

Table 6: simulations with the original free-energy model

Simulation	ρα	ρβ	b=-a	Γ	κ	σ	$\frac{\nu_\alpha}{\nu_\beta}$	$\frac{\rho_\alpha}{\rho_\beta}$	force
1	1	1	0.01	10	1.00E-05	2.98E-04	1	1	0.0001
2	1	1	0.01	10	1.00E-05	2.98E-04	10	1	0.0001
3	1	1	0.01	10	1.00E-05	2.98E-04	100	1	0.0001
4	2	1	0.01	10	1.00E-05	2.98E-04	1	2	0.0001
5	10	1	0.01	10	1.00E-05	2.98E-04	1	10	0.0001

The following figure shows the density profile across the channel for the case #1.

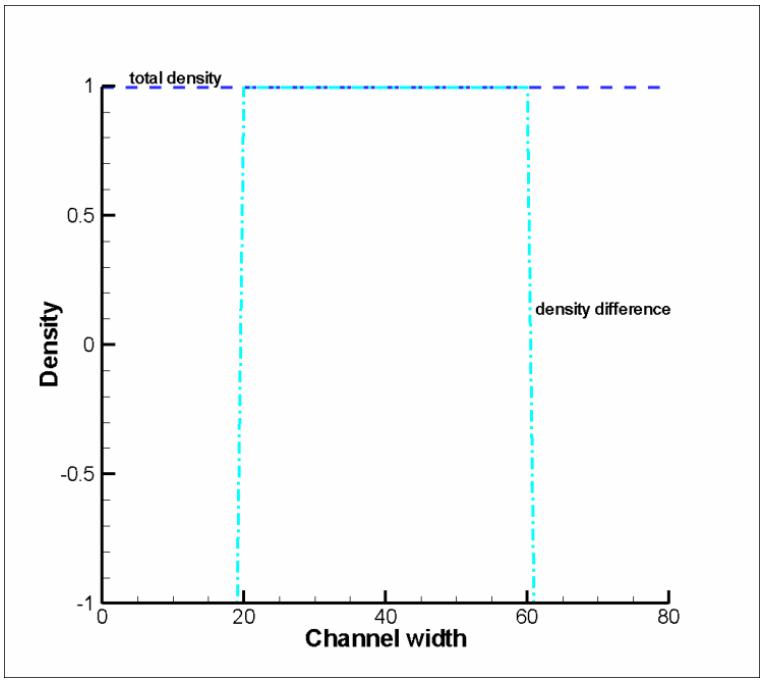

Figure 28: density profile across the channel (free-energy model)

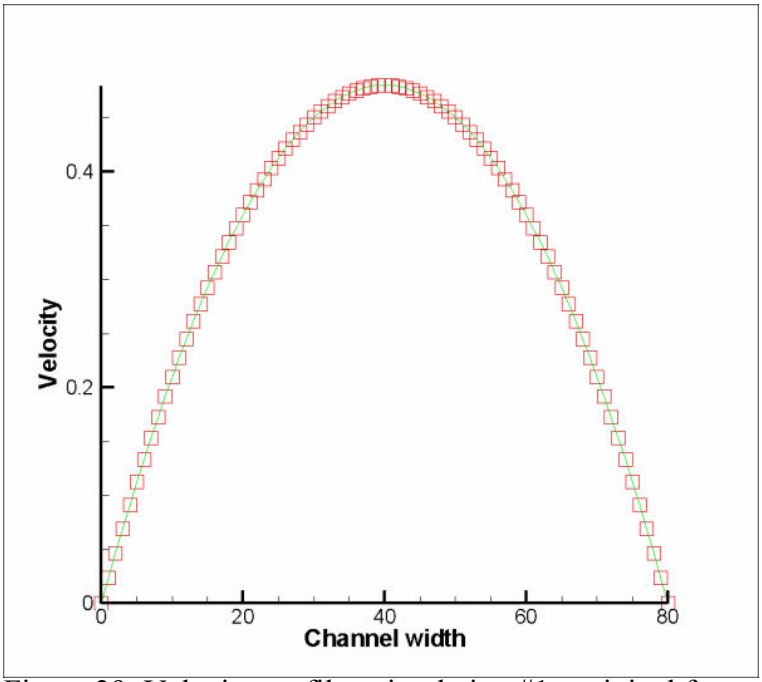

Figure 29: Velocity profile - simulation #1 - original free-energy model

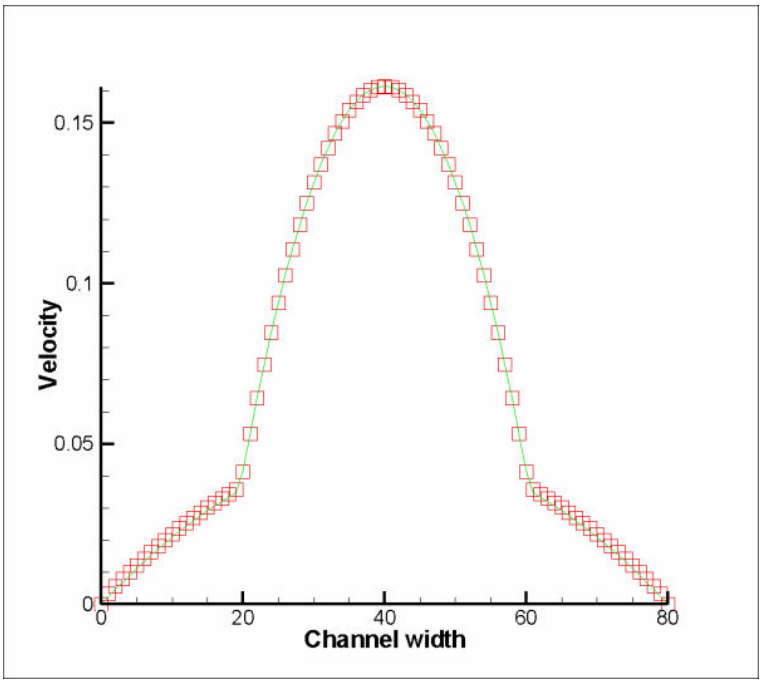

Figure 30: Velocity profile - simulation #2 - original free-energy model

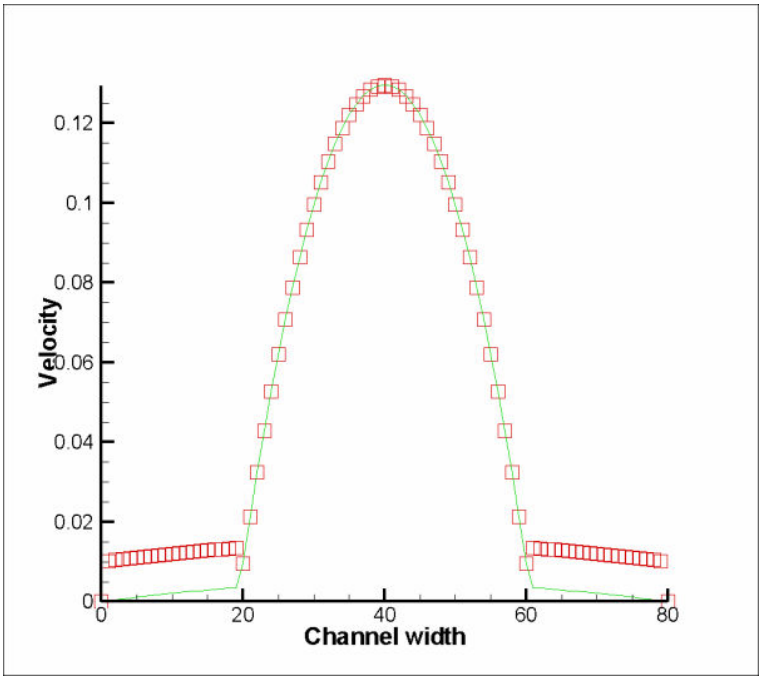

Figure 31: Velocity profile - simulation #3 - original free-energy model

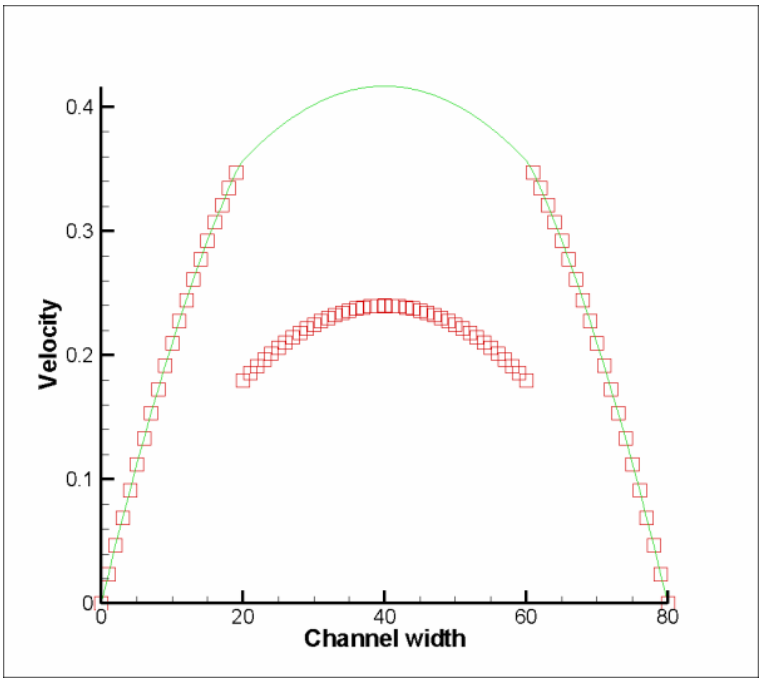

Figure 32: Velocity profile - simulation #4 - original free-energy model

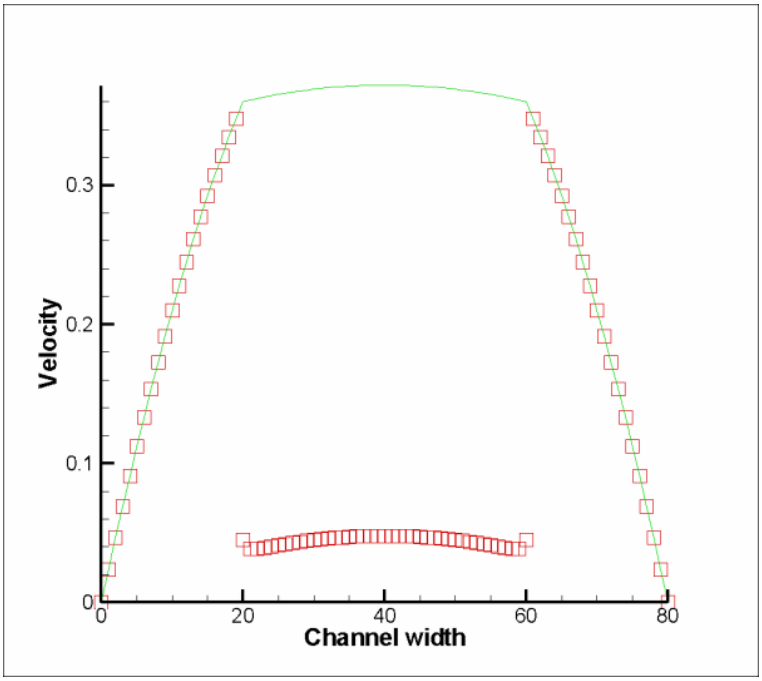

Figure 33: Velocity profile - simulation #5 - original free-energy model

We simulated the following cases using the method based on the free energy approach for large density ratios developed by Zheng:

Table 7: simulations with the free-energy model for large density ratios

Simulation#	ρα	ρβ	Γ	κ	A	W	να/νβ	ρα/ρβ	force
6	10	1	10	3.70E-03	9.14E-05	2	1	10	0.0001
7	100	1	100	3.06E-05	6.25E-09	2	1	100	0.0001

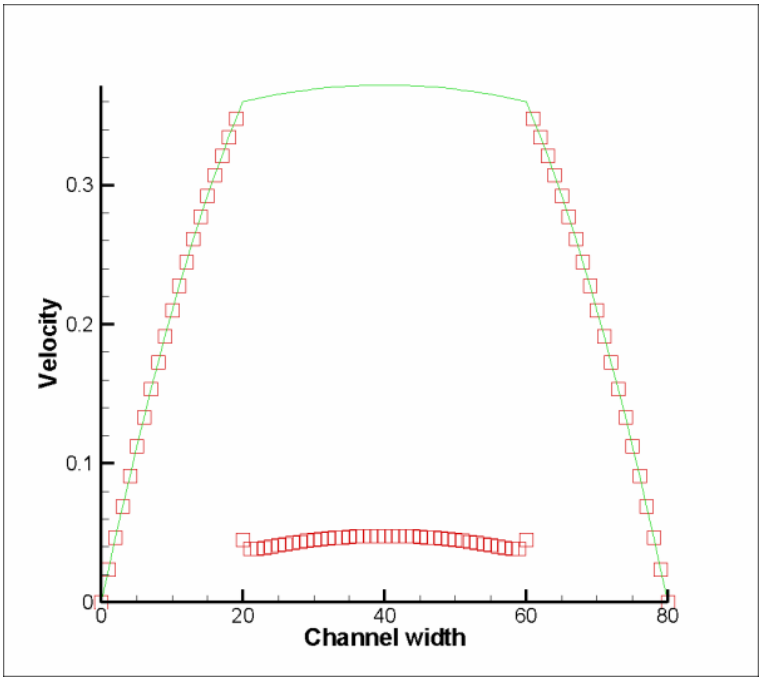

Figure 34: Velocity profile - simulation #6 - free-energy model for large density ratio

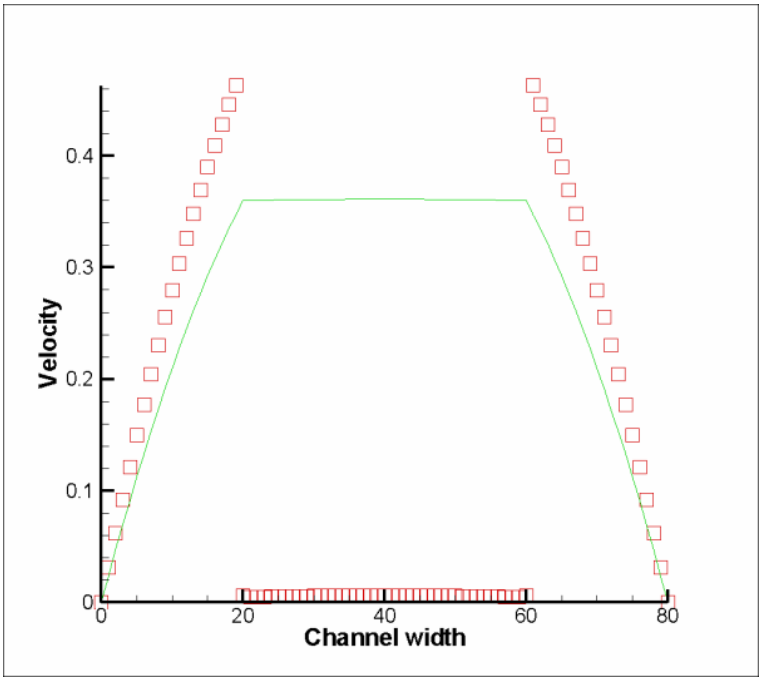

Figure 35: Velocity profile - simulation #7- free-energy model for large density ratio

When the two phases have the same density but different viscosities, the comments made for the color-fluid model apply but the accuracy is slightly different. The following table sums up the results when the two fluids have diferent viscosities.

Table 8: results with free-energy model - different viscosities

case#	average error	maximum error	error at the interface
1	0.0512	0.4223	0.0252
2	3.697	39.4513	0.0882
3	391.0958	4197.7	285.4863

If the two phases have different densities, we observe a large discontinuity at the interface. This discontinuity increases as the density ratio increases. The model by Zheng is more robust and allows us to simulate flows with high density ratios but does not improve continuity at the interface. The problem highlighted in section 3 for the case of

the color-fluid model when the two fluids have different densities applies to both free-energy models (original free-energy model and free-energy model for large density ratios): when computing the macroscopic velocity u, $\sum f_i e_i$ is divided by ρ, which inevitably creates, at the interface, a discontinuity proportional to ρ_α / ρ_β.

Results obtained with the mean-field theory model

We simulated the following cases:

Table 9: simulations with the mean-field theory model

Simulation	RT	a	κ	τα	τα	ρα	ρβ	$\frac{\nu_\alpha}{\nu_\beta}$	$\frac{\rho_\alpha}{\rho_\beta}$	force
1	0.33333	4	0	1	1	0.5	0.5	1	1	0.0001
2	0.33333	4	0	1.03636	0.58007	0.5	0.5	6.7	1	0.0001
3	0.33333	4	0	5.9	0.77851	0.5	0.5	19.4	1	0.0001
4	0.33333	4	0	1	1	0.5	0.45	1	1.11	0.0001
5	0.33333	4	0	1	1	0.5	0.25	1	2	0.0001

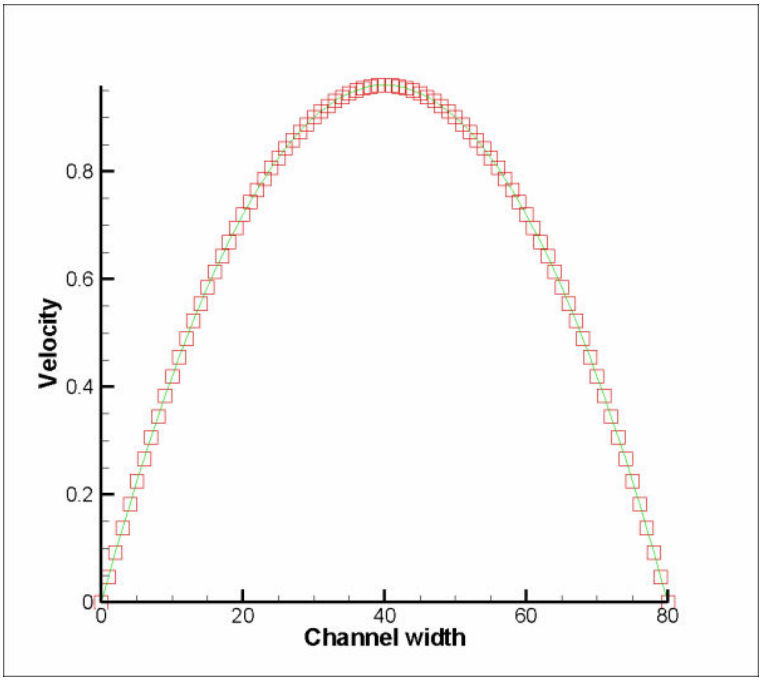

Figure 36: Velocity profile - simulation #1 - mean-field theory model

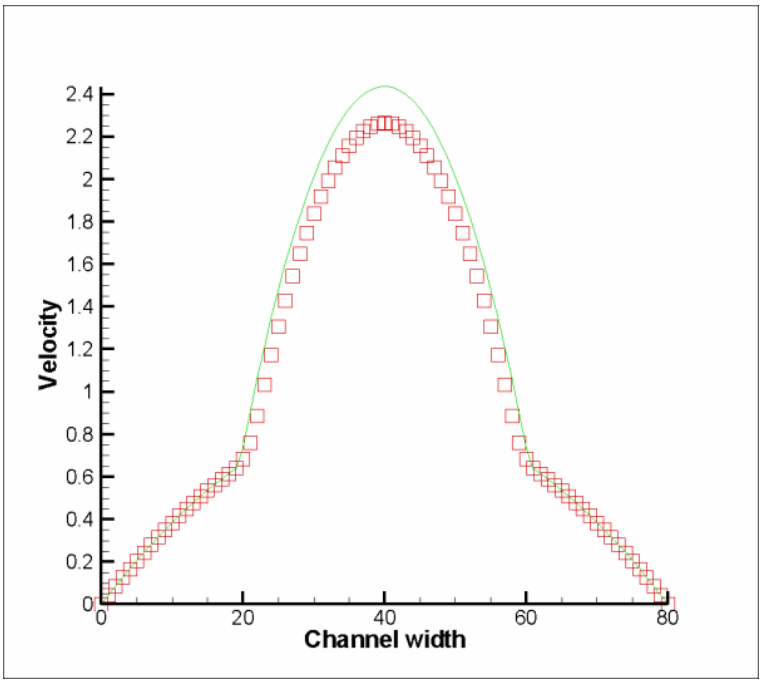

Figure 37: Velocity profile - simulation #2 - - mean-field theory model

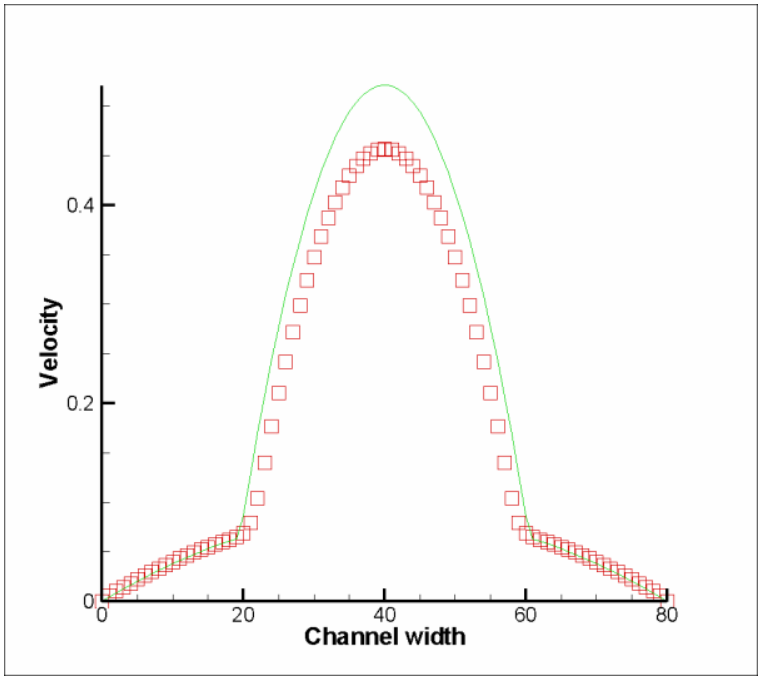

Figure 38: Velocity profile - simulation #3 - - mean-field theory model

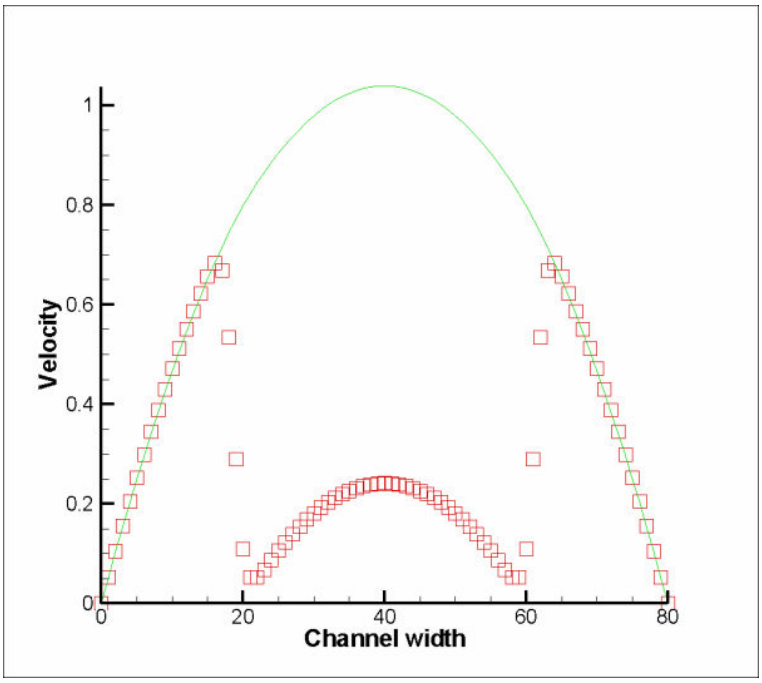

Figure 39: Velocity profile - simulation #4 - - mean-field theory model

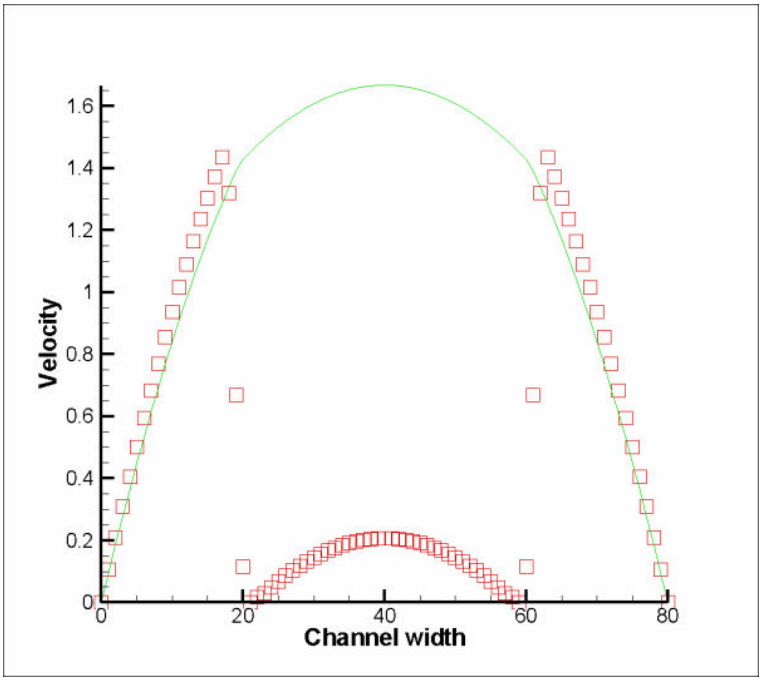

Figure 40: Velocity profile - simulation #5 - - mean-field theory model

When the two fluids have different viscosities, the interface tends to move slightly, which modifies the initial conditions, but our simulations take care of this phenomenon by reevaluating the viscosity and the width of the each phase. The results show very good agreement in the high viscosity phase (outer layer) with the analytical solution even for high-viscosity ratios. However, we observe a discrepancy in the low viscosity phase (inner layer) and the error is greatest on the inner side of the interface. The following table sums up the results when the two fluids have diferent viscosities.

Table 10: results with mean-field theory model - different viscosities

case#	average error	maximum error	error at the interface
1	0.0769	0.6331	0.0419
2	5.1591	16.3068	16.3068
3	13.8587	45.2422	30.4008

When the two fluids have diferent densities, we observe a large discontinuity, which increases as the density ratio increases. We notice that the discontinuity is larger than the one obtained with the three other models. Hence, we cannot build a correct velocity profile by adding $\frac{\rho_\beta}{\rho_\alpha} V_{\text{interf}}$ to the velocity in the inner layer.

Conclusion

This chapter presents a review of the main lattice-Boltzmann methods for immiscible two-phase flow: color-fluid model, interparticle-potential model, free-energy model, and mean-field theory model. These models can lead to discontinuity at the interface between two fluids when the two fluids have different viscosities or different densities. We evaluated the ability of these four models to simulate two-phase Poiseuille flow and to maintain continuity at the interface.

When the two fluids have different densities, discontinuity is inevitable because the solution for f_i is independent of the sound speed or the density. Therefore, the macroscopic velocity, which is proportional to $1/\rho$ undergoes a jump at the interface.

When the two fluids have different viscosities, the free-energy model gives accurate results, except for high-viscosity ratios (M=100) for which we observe a discontinuity at the interface. For low-viscosity ratios, the color fluid model gives accurate results with either a BGK or a TRT collision operator but if the viscosity ratio is too high (M = 100), only a TRT collision operator can guarantee continuity at the interface. The discontinuities obtained with the free-energy model and the color-fluid model (BGK collision operator) for M equals 100 are similar (286%). The interparticle-potential model leads to a discrepancy at the interface even for low-viscosity ratios. Moreover, this model is not purely immiscible and the physical properties of the two phases do not remain constant (viscosity and density). The mean-field theory model gives accurate results for the high-viscosity phase but poor results for the low-viscosity phase. However, no discontinuity is observed at the interface for viscosity ratios up to 19.

CHAPTER 4

3D IMPLEMENTATION OF THE COLOR-FLUID MODEL

Introduction

This chapter presents a 3D implementation of the most recent version of the color-fluid model, which includes the improvements proposed by Lishchuk [9] and Latva-Kokko [10]. The objective is to assess the accuracy and consistency of this model through different test cases. Two tests of coherence, the free deformation of a cubic bubble and the coalescence of two spherical bubbles, verify that the interaction between two fluids is properly modeled. The Laplace bubble test case allows assessment of the accuracy of the scheme used to apply the surface tension effect. The two-phase Poiseuille flow test case (chapter 3) allows study of the problem of continuity at the interface between the two fluids. Finally, the simulation of the free rise of a bubble in a quiescent fluid is a good way to evaluate the ability of the model to simulate bubble dynamics.

Validation of the code

3D implementation

We adapted the method presented in section 2 “color fluid model” to 3D using a lattice with nineteen velocities (3D19Q). The 3D19Q model has the following set of discrete velocities and weighting factors

$$e_i = \begin{cases} (0;0;0) & & & i=0 \\ (\pm 1;0;0)c & (0;\pm 1;0)c & (0;0;\pm 1)c & i=1,2,...,6 \\ (\pm 1;\pm 1;0)c & (\pm 1;0;\pm 1)c & (0;\pm 1;\pm 1)c & i=7,8,...,18 \end{cases} \tag{52}$$

$$w_i = \begin{cases} 1/3 & i = 0 \\ 1/18 & i = 1,2,...,6 \\ 1/36 & i = 7,8,...,18 \end{cases} . \quad (53)$$

We also need to redefine the coefficients r_i that appear in the definition of the equilibrium distribution function $f_i^{\alpha\ eq} = \rho w_i \left[r_i + 3e_i.v + \frac{9}{2}(e_i.v)^2 - \frac{3}{2}v^2 \right]$ and allow conservation of momentum near the interface between the two fluids. The 3D19Q model requires:

$$r_i = \begin{cases} \dfrac{\rho_\beta}{\rho_\alpha} & i = 0 \\ 3 - \dfrac{2\rho_\beta}{\rho_\alpha} & i = 1,2...18 \end{cases} \quad (54)$$

Coalescence of two spherical bubbles, free deformation of a cubic bubble

To ensure that the surface tension effect is correctly implemented in the 3D model, we consider two tests of coherence (TC). The first test case simulates the coalescence of two bubbles. At t=0, two identical bubbles are in contact, but as time goes by, they tend to fuse into a single bubble. The second simulates the deformation of a cubic bubble, which becomes a static spherical bubble.

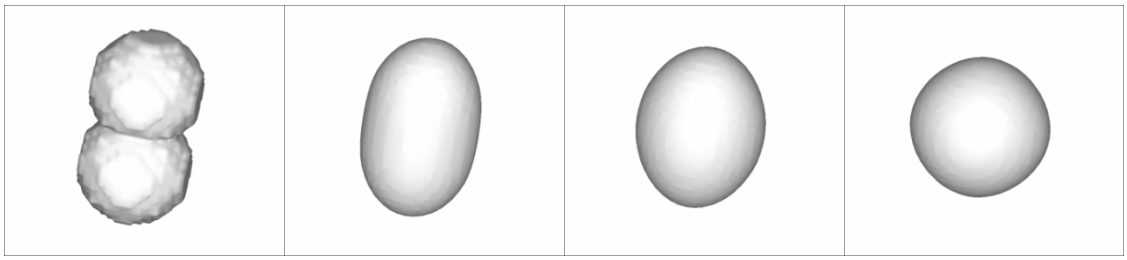

Figure 41: Results of Test Case 1- Coalescence of two identical spherical bubbles

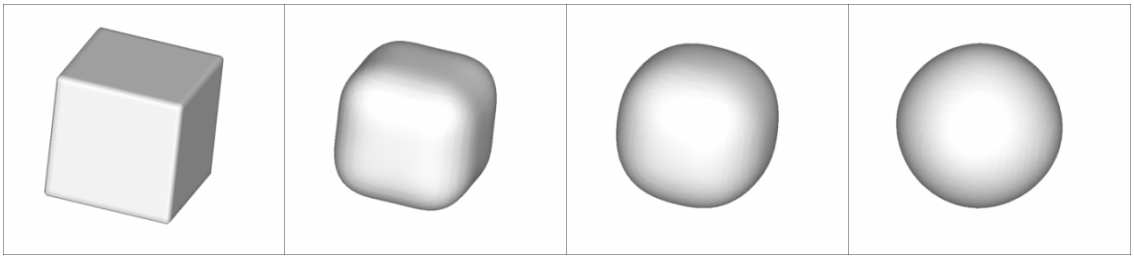

Figure 42: Results of Test Case 2 - Free deformation of a cubic bubble

In both cases, we observe a coherent deformation from the initial state to the final static bubble, which indicates that the surface tension effect is qualitatively properly modeled.

Laplace bubble test

The Laplace bubble test allows us to check that the surface tension induces a correct pressure difference at the interface between the two fluids. This test consists of a static spherical bubble of β-fluid immersed in a quiescent α-fluid. The pressure difference at the interface is controlled by the Laplace-Young equation $\Delta p = \frac{2\sigma}{R}$ in which R is the radius of the bubble.

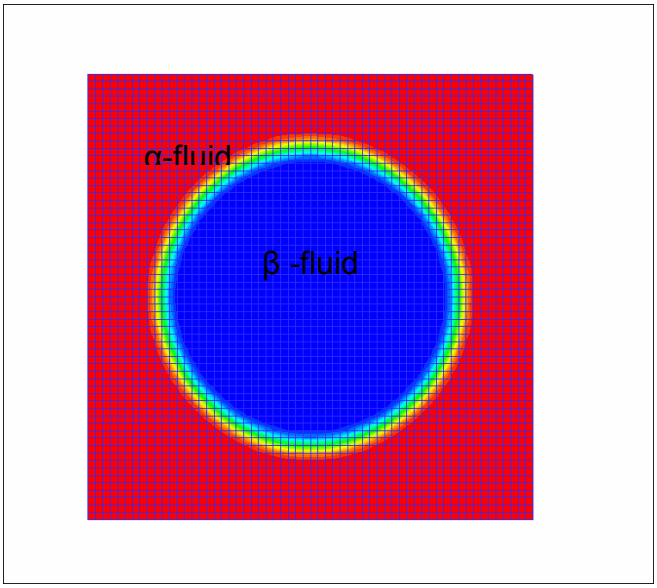

Figure 43: configuration – Laplace bubble test

This test case is a "PA" test case (physical test-case compared with an analytical solution). We compare the pressure difference given by the Laplace-Young equation to the pressure jump simulated by our model. In the lattice-Boltzmann method, pressure is related to density by

$$\begin{cases} p_\alpha = \rho_\alpha c_\alpha{}^2, \\ p_\beta = \rho_\beta c_\beta{}^2. \end{cases} \tag{55}$$

For the first series of simulations, the surface tension value is fixed at $\sigma = 0.01$. We simulate this test case for bubbles with different radii. We simulate three more cases to verify results with different values of surface tension or density differences.

Results:

Table 11: results of the Laplace bubble test

ρα	ρβ	σ supplied	R computed	ΔP	ΔP theory	σ computed	error (%)
0.99958	1.00247	0.01	20.399	0.000964	0.000980	**0.009832**	**1.677**
0.99960	1.00343	0.01	15.415	0.001278	0.001297	**0.009848**	**1.525**
0.99952	1.00431	0.01	12.355	0.001597	0.001619	**0.009868**	**1.324**
0.99967	1.00540	0.01	10.310	0.001911	0.001940	**0.009851**	**1.491**
0.99979	1.00708	0.01	8.113	0.002427	0.002465	**0.009847**	**1.530**
1.98481	0.99739	0.01	11.873	0.001662	0.001684	**0.009869**	**1.312**
1.98582	0.99340	0.001	12.162	0.000163	0.000164	**0.000992**	**0.776**
9.41521	0.94793	0.01	9.248	0.002135	0.002163	**0.009874**	**1.261**

The following graph shows the linear relationship between the curvature and the pressure jump. Our results match the Laplace-Young equation with less than a 2% error.

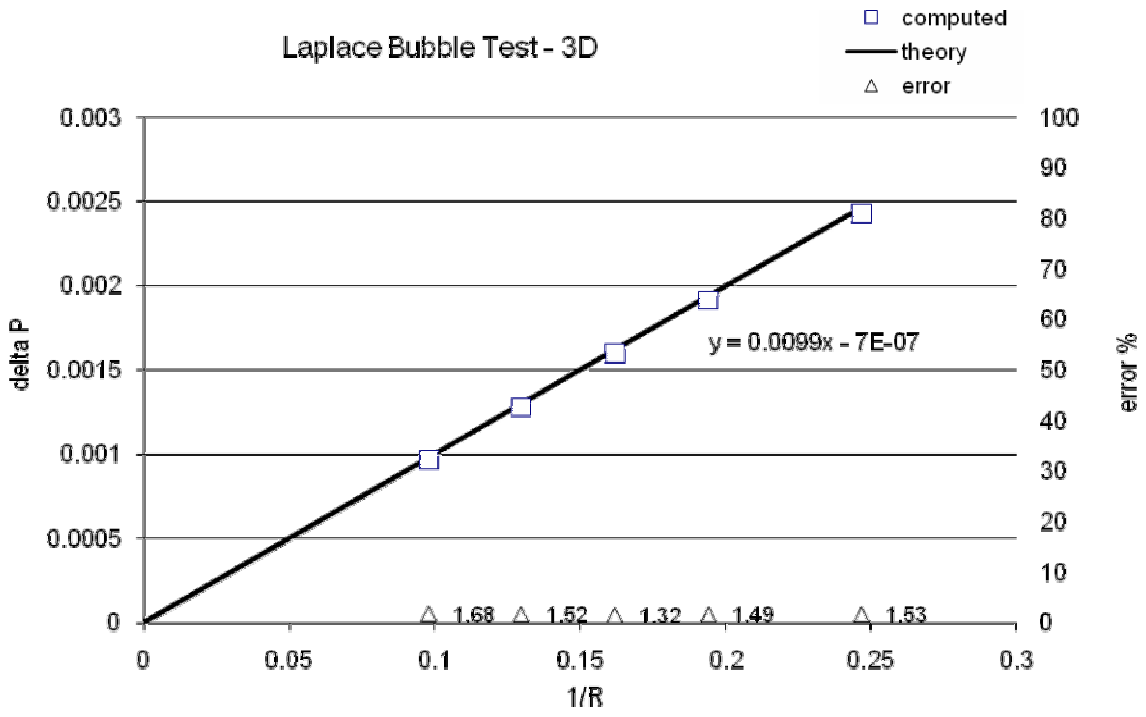

Figure 44: results – Laplace bubble test

Free rise of a bubble in a quiescent viscous fluid

A classical test case used to validate two-phase flow models is the simulation of a bubble rising in a viscous fluid. We release a spherical bubble in a viscous, quiescent fluid and we impose a gravity force. Due to buoyancy forces, the bubble will tend to rise. When the bubble reaches terminal conditions (steady state), we can assume that its shape is fixed and that its velocity is constant. The shape and the terminal velocity of the bubble are the two key parameters. In order to analyze the ability and accuracy of our model to simulate bubble dynamics, we compare our results with those obtained by Ismail Oguz Kurtoglu and Ching-Long Lin [36], and Takada et al. [37].

The flow is characterized by three dimensionless parameters, the Eotvos number, the Morton number, and the Reynolds number:

$$Eo = \frac{g\Delta\rho d_e^{\,2}}{\sigma} \qquad Mo = \frac{g\Delta\rho\mu^4}{\rho^2\sigma^3} \qquad \mathrm{Re} = \frac{\rho d_e Ut}{\mu}, \tag{56}$$

where d_e is the effective diameter, ρ is the density of the surrounding fluid, Δρ is the density difference between the two phases. The Eotvos number is the dimensionless size of the bubble, the Morton number characterizes the fluid properties of the surrounding phase, and the Reynolds number determines the flow field around the bubble.

The density ratio between the two fluids α and β is the biggest issue in the lattice Boltzmann model. Whereas in nature we can observe two-phase systems with a density ratio, from 1 to 10,000, our model requires low-density ratios (1-20). We simulated two cases with the following parameters:

Table 12: simulation parameters for the test case "Free rise of a bubble"

Case	d	g	σ	τα = τβ	να = νβ	ρα/ρβ	Eo	M	τ^*
1	20	0.00031	0.00521	0.875	0.125	2.45	20	0.905919	0.75
2	20	0.001551	0.00521	0.875	0.125	2.45	100	4.529595	0.75

Table 13: terminal velocity of a bubble rising freely in a quiescent viscous fluid"

Case	Ut – LBM present model	Ut –LBM Kurtoglu	Ut – LBM Takada	Ut – VOF Takada
1	2.60E-02	2.24E-02	2.17E-02	2.15E-02
2	5.10E-02	5.43E-02	5.03E-02	5.05E-02

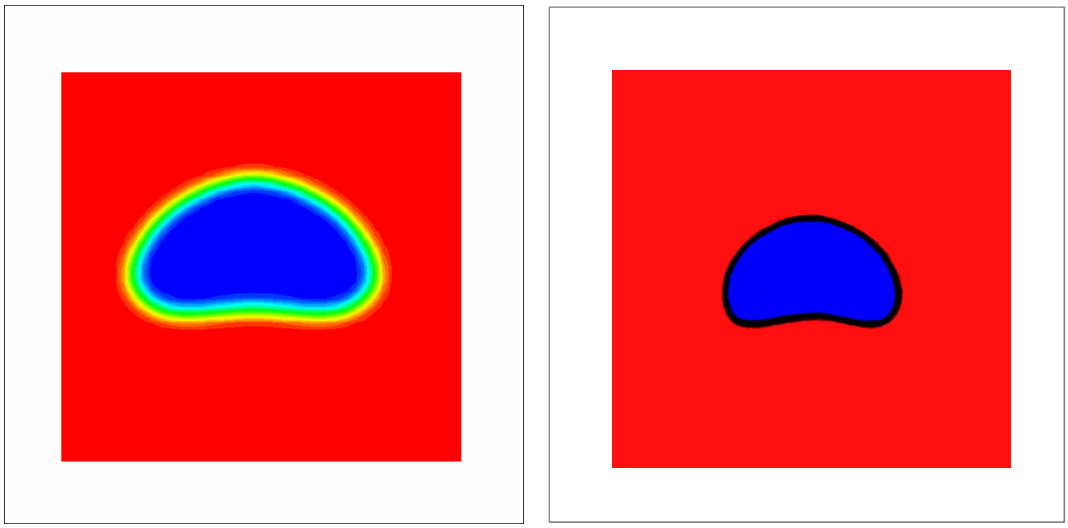

Figure 45: terminal shape – case 1 – present model (left) and Kurtoglu and Lin (right)

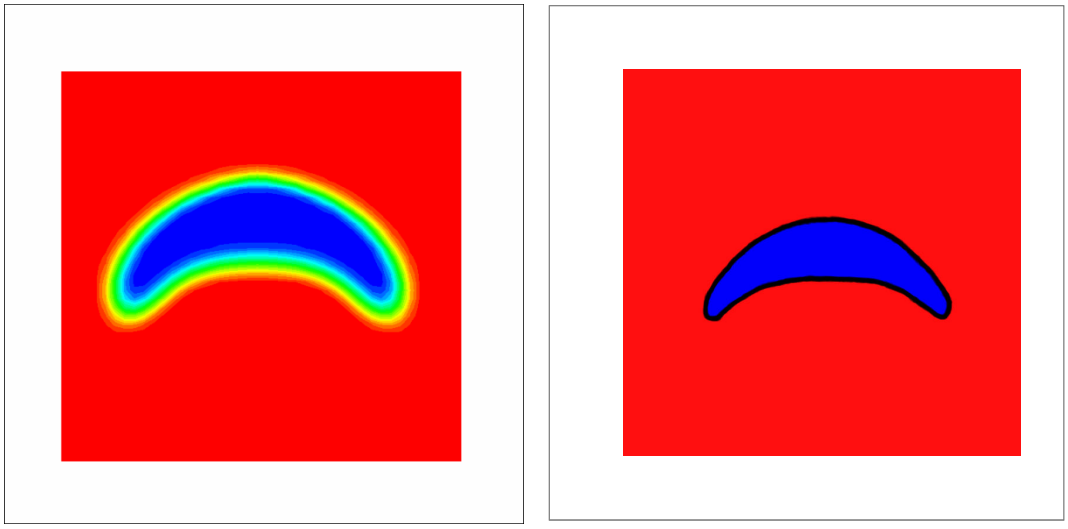

Figure 46: terminal shape – case 2 – present model (left) and Kurtoglu and Lin (right)

Our results are similar to those obtained by Ismail Oguz Kurtoglu and Ching-Long Lin [36], and Takada et al. [37].

Conclusion

This chapter presents the most recent version of the color-fluid method, which improves on the Gunstensen model in two ways: first, by directly applying the surface tension at the interface, and secondly, by using the improved segregation process developed by Latva-Kokko. In order to assess the accuracy of the present method, four test cases have been run: coalescence of two spherical bubbles and free deformation of a cubic bubble, Laplace bubble test, Poiseuille two-phase flow (chapter 3), and the free rise of a bubble in a quiescent viscous fluid. They all show good agreement with the references used. Indeed, the surface tension applied at the interface creates a pressure difference that follows the Laplace-Young law with less than a 2% error (Laplace bubble test). Moreover, the present model is able to simulate stratified two-phase flow and guarantees continuity at the interface as long as the two fluids have the same densities (Poiseuille two-phase flow - chapter 3). In addition, simulations show that the present model accurately captures the physics of bubble dynamics (free rise of a bubble in a quiescent viscous fluid).

CHAPTER 5

GENERAL CONCLUSION

This thesis presents a review of the lattice-Boltzmann approaches for analyzing immiscible two-phase flow. The four main methods are presented in detail: color-fluid model, interparticle-potential model, free-energy model, mean-field theory model, and recent improvements on these methods.

In chapter 3, we compare the ability of these methods to maintain continuity at the interface between two fluids. When the two fluids have different densities, discontinuity is inevitable and the macroscopic velocity undergoes a jump at the interface proportional to ρ_α / ρ_β. When the two fluids have different viscosities, the four models behave differently. The free-energy model gives accurate results, except for high-viscosity ratios (M=100) for which we observe a discontinuity at the interface, which is comparable to the discontinuity obtained with the color-fluid model (BGK collision operator). The color fluid model gives accurate results with either a BGK or a TRT collision operator for low-viscosity ratios, but if the viscosity ratio is too high (M = 100), only a TRT collision operator can guarantee continuity at the interface. The interparticle-potential model leads to a discrepancy at the interface even for low-viscosity ratios. The mean-field theory model gives accurate results for the high-viscosity phase but poor results for the low-viscosity phase.

In chapter 4, we present a 3D implementation of the color-fluid model and we assess the capability of this model by simulating four test cases: coalescence of two spherical bubbles and free deformation of a cubic bubble, Laplace bubble test, Poiseuille

two-phase flow (chapter 3), and the free rise of a bubble in a quiescent viscous fluid. They all show fair agreement with the references used. Indeed, the results verify the Laplace law with a 2% error, continuity is satisfied for stratified flow (Poiseuille flow) even for high viscosity ratios, and the final shape and velocity of a rising bubble are predicted with accuracy.

APPENDIX A

EXPLANATION OF THE DISCONTINUITY FOR THE CASE $\frac{\rho_\alpha}{\rho_\beta} \neq 1$

We start from the continuous tensor stress defined as [38]

$$\sigma_{kl} = -\frac{1}{6\tau}\rho\delta_{ij} - \left(1-\frac{1}{2\tau}\right)\sum_i \left(e_{ik}-u_k\right)\left(e_{il}-u_l\right) f_i \,. \tag{57}$$

For the parallel two-phase Poiseuille flow in the channel considered here, the only non-diagonal term in the stress tensor (i.e., shear stress term) that is not zero is σ_{xy} , where *x* is the streamwise direction.

For velocity to be continuous at the interface, it follows that $\left(e_{ik}-u_x\right)\left(e_{il}-u_y\right) = a_i$ is continuous. Continuity of the shear stress can be expressed as

$$\left(1-\frac{1}{2\tau}\right)\sum_i a_i f_i^{high\ density\ phase} = \left(1-\frac{1}{2\tau}\right)\sum_i a_i f_i^{low\ density\ phase} \,. \tag{58}$$

Since ρ is discontinuous, we have

$$\sum_i f_i^{high\ density\ phase} = \frac{\rho_{high\ density\ phase}}{\rho_{low\ density\ phase}}\sum_i f_i^{low\ density\ phase} \tag{59}$$

Which leads to

$$\sum_i a_i f_i^{high\ density\ phase} = \frac{\rho_{high\ density\ phase}}{\rho_{low\ density\ phase}}\sum_i a_i f_i^{low\ density\ phase} \tag{60}$$

The two fluids have the same viscosity (same τ).

$$\left(1-\frac{1}{2\tau}\right)\sum_i a_i f_i^{high\ density\ phase} = \left(1-\frac{1}{2\tau}\right)\frac{\rho_{high\ density\ phase}}{\rho_{low\ density\ phase}}\sum_i a_i f_i^{low\ density\ phase} \tag{61}$$

This contradicts the continuity of the shear stress (58), so our assumption of continuous velocity is not valid, and the discontinuity is scaled with $\frac{\rho_{high\ density\ phase}}{\rho_{low\ density\ phase}}$. This shows that

fundamentally, the shear stress and velocity cannot simultaneously be continuous at the interface when the density of each phase is different.

REFERENCES

1. Gunstensen, A.K., et al., *Lattice Boltzmann model of immiscible fluids.* Physical Review A (Statistical Physics, Plasmas, Fluids, and Related Interdisciplinary Topics), 1991. **43**(8): p. 4320-7.

2. Shan, X. and H. Chen, *Lattice Boltzmann model for simulating flows with multiple phases and components.* Physical Review E. Statistical Physics, Plasmas, Fluids, and Related Interdisciplinary Topics, 1993. **47**(3): p. 1815.

3. Shan, X.W. and H.D. Chen, *Simulation of nonideal gases and liquid-gas phase-transitions by the lattice-Boltzmann equation.* Physical Review E, 1994. **49**(4): p. 2941-2948.

4. Swift, M.R., et al., *Lattice Boltzmann simulations of liquid-gas and binary fluid systems.* Physical Review E. Statistical Physics, Plasmas, Fluids, and Related Interdisciplinary Topics, 1996. **54**(5): p. 5041.

5. He, X.Y., X.W. Shan, and G.D. Doolen, *Discrete Boltzmann equation model for nonideal gases.* Physical Review E, 1998. **57**(1): p. R13-R16.

6. Rothman, D.H. and J.M. Keller, *Immiscible cellular-automaton fluids.* Journal of Statistical Physics, 1988. **52**(3-4): p. 1119-27.

7. Grunau, D., S. Chen, and K. Eggert, *A lattice Boltzmann model for multiphase fluid flows.* Physics of Fluids A (Fluid Dynamics), 1993. **5**(10): p. 2557-62.

8. Reis, T. and T.N. Phillips, *Lattice Boltzmann model for simulating immiscible two-phase flows.* Journal of Physics A: Mathematical and Theoretical, 2007. **40**(14): p. 4033-53.

9. Lishchuk, S.V., C.M. Care, and I. Halliday, *Lattice Boltzmann algorithm for surface tension with greatly reduced microcurrents.* Physical Review E - Statistical, Nonlinear, and Soft Matter Physics, 2003. **67**(3 2): p. 036701-1.

10. Latva-Kokko, M. and D.H. Rothman, *Diffusion properties of gradient-based lattice Boltzmann models of immiscible fluids.* Physical Review E - Statistical, Nonlinear, and Soft Matter Physics, 2005. **71**(5): p. 056702.

11. Kang, Q., D. Zhang, and S. Chen, *Immiscible displacement in a channel: Simulations of fingering in two dimensions.* Advances in Water Resources, 2004. **27**(1): p. 13-22.

12. Chin, J., E.S. Boek, and P.V. Coveney. *Lattice Boltzmann simulation of the flow of binary immiscible fluids with different viscosities using the Shan-Chen microscopic interaction model*. 2002. Cargese, France: R. Soc.

13. Kang, Q., D. Zhang, and S. Chen, *Displacement of a two-dimensional immiscible droplet in a channel.* Physics of Fluids, 2002. **14**(9): p. 3203-3214.

14. Zhang, R., et al., *Surface tension effects on two-dimensional two-phase Kelvin-Helmholtz instabilities.* Advances in Water Resources, 2001. **24**(3-4): p. 461-478.

15. Yuan, P. and L. Schaefer, *Equations of state in a lattice Boltzmann model.* Physics of Fluids, 2006. **18**(4): p. 042101.

16. Qin, R.S., *Mesoscopic interparticle potentials in the lattice Boltzmann equation for multiphase fluids.* Physical Review E - Statistical, Nonlinear, and Soft Matter Physics, 2006. **73**(6): p. 066703.

17. Falcucci, G., et al., *Lattice boltzmann models with mid-range interactions.* Communications in Computational Physics, 2007. **2**(6): p. 1071-84.

18. Chibbaro, S., et al., *Lattice Boltzmann models for nonideal fluids with arrested phase-separation.* Physical Review E - Statistical, Nonlinear, and Soft Matter Physics, 2008. **77**(3): p. 036705.

19. Orlandini, E., M.R. Swift, and J.M. Yeomans, *A lattice Boltzmann model of binary-fluid mixtures.* Europhysics Letters, 1995. **32**(6): p. 463-8.

20. Holdych, D.J., et al. *An improved hydrodynamics formulation for multiphase flow lattice-Boltzmann models*. 1998. Oxford, UK: World Scientific.

21. Inamuro, T., N. Konishi, and F. Ogino. *A Galilean invariant model of the lattice Boltzmann method for multiphase fluid flows using free-energy approach*. 2000. Tokyo, Japan: Elsevier.

22. Kalarakis, A.N., V.N. Burganos, and A.C. Payatakes, *Galilean-invariant lattice-Boltzmann simulation of liquid-vapor interface dynamics.* Physical Review E - Statistical, Nonlinear, and Soft Matter Physics, 2002. **65**(5): p. 056702.

23. Zheng, H.W., C. Shu, and Y.T. Chew, *A lattice Boltzmann model for multiphase flows with large density ratio.* Journal of Computational Physics, 2006. **218**(1): p. 353-371.

24. Inamuro, T., et al., *A lattice Boltzmann method for incompressible two-phase flows with large density differences.* Journal of Computational Physics, 2004. **198**(2): p. 628-44.

25. He, X., S. Chen, and R. Zhang, *A lattice Boltzmann scheme for incompressible multiphase flow and its application in simulation of Rayleigh-Taylor instability.* Journal of Computational Physics, 1999. **152**(2): p. 642-63.

26. He, X., et al., *On the three-dimensional Rayleigh-Taylor instability.* Physics of Fluids, 1999. **11**(5): p. 1143-1152.

27. Lee, T. and C.L. Lin, *A stable discretization of the lattice Boltzmann equation for simulation of incompressible two-phase flows at high density ratio.* Journal of Computational Physics, 2005. **206**: p. 16-47.

28. Frisch, U., B. Hasslacher, and Y. Pomeau, *Lattice-gas automata for the Navier-Stokes equation.* Physical Review Letters, 1986. **56**(14): p. 1505-8.

29. Succi, S., ed. *The Lattice Boltzmann Equation for Fluid Dynamics and Beyond: For Fluid Dynamics and Beyond*. 2001, Oxford University Press. 288

30. Nourgaliev, R.R., et al., *The lattice Boltzmann equation method: Theoretical interpretation, numerics and implications.* International Journal of Multiphase Flow, 2003. **29**(1): p. 117-69.

31. Brackbill, J.U., D.B. Kothe, and C. Zemach, *A continuum method for modeling surface tension.* Journal of Computational Physics, 1992. **100**(2): p. 335-54.

32. Halliday, I., et al., *Improved simulation of drop dynamics in a shear flow at low Reynolds and capillary number.* Physical Review E (Statistical, Nonlinear, and Soft Matter Physics), 2006. **73**(5): p. 56708-1.

33. Ginzburg, I., *Lattice Boltzmann modeling with discontinuous collision components: hydrodynamic and advection-diffusion equations.* Journal of Statistical Physics, 2007. **126**(1): p. 157-206.

34. Xu, A., G. Gonnella, and A. Lamura, *Phase-separating binary fluids under oscillatory shear.* Physical Review E, 2003. **67**(5 2): p. 056105-1.

35. Langaas, K. and S. Nilsson, *Pore-scale simulations of disproportionate permeability reducing gels.* Journal of Petroleum Science and Engineering, 2000. **25**(3): p. 167-186.

36. Kurtoglu, I.O. and L. Ching-Long, *Lattice Boltzmann study of bubble dynamics.* Numerical Heat Transfer, Part B (Fundamentals), 2006. **50**(4): p. 333-51.

37. Takada, N., et al., *Numerical simulation of two- and three-dimensional two-phase fluid motion by lattice Boltzmann method.* Computer Physics Communications, 2000. **129**(1): p. 233-246.

38. Huabing, L., et al., *Force evaluations in lattice Boltzmann simulations with moving boundaries in two dimensions.* Physical Review E (Statistical, Nonlinear, and Soft Matter Physics), 2004. **70**(2): p. 26701-1.